FDL-TDR-64-130

AN EXPERIMENTAL STUDY OF REAL GAS EFFECTS ON SHOCK DETACHMENT DISTANCES AND SHOCK SHAPES FOR A FAMILY OF BLUNT AXISYMMETRIC BODIES

TECHNICAL DOCUMENTARY REPORT No. FDL-TDR-64-130

OCTOBER 1964

AIR FORCE FLIGHT DYNAMICS LABORATORY
RESEARCH AND TECHNOLOGY DIVISION
AIR FORCE SYSTEMS COMMAND
WRIGHT-PATTERSON AIR FORCE BASE, OHIO

Project No. 1426, Task No. 142604

(Prepared under Contract No. AF 33(657)-10416 by The Aerodynamic Laboratory, The Ohio State University Research Foundation, Columbus, Ohio; Bruce C. Graber, Author)

NOTICES

When Government drawings, specifications, or other data are used for any purpose other than in connection with a definitely related Government procurement operation, the United States Government thereby incurs no responsibility nor any obligation whatsoever; and the fact that the Government may have formulated, furnished, or in any way supplied the said drawings, specifications, or other data, is not to be regarded by implication or otherwise as in any manner licensing the holder or any other person or corporation, or conveying any rights or permission to manufacture, use, or sell any patented invention that may in any way be related thereto.

Qualified requesters may obtain copies of this report from the Defense Documentation Center (DDC), (formerly ASTIA), Cameron Station, Bldg. 5, 5010 Duke Street, Alexandria, Virginia, 22314.

This report has been released to the Office of Technical Services, U.S. Department of Commerce, Washington 25, D. C., in stock quantities for sale to the general public.

Copies of this report should not be returned to the Research and Technology Division, Wright-Patterson Air Force Base, Ohio, unless return is required by security considerations, contractual obligations, or notice on a specific document.

300 - December 1964 - 448-16-409

B

FOREWORD

This report (Interim Technical Report No. 4, RF Project 1580) was prepared for The Ohio State University Research Foundation on Contract No. AF 33(657)-10416, "Research on Similarity Parameters Relating Model Tests in High-Enthalpy Hypersonic Wind Tunnels to Corresponding Full-Scale Flight Conditions." The work reported herein was performed during the period 1 January 1963 to 1 February 1964 on Project 1426, "Experimental Simulation of Flight Mechanisms," Task 142604, "Theory of Dynamic Simulation of Flight Environments." The project was monitored by Mr. F. J. A. Huber, of the Air Force Flight Dynamics Laboratory, Research and Technology Division.

ABSTRACT

Shock shapes and detachment distances for a group of spherical-nosed bodies are presented and analyzed in terms of their dependence on several of the flow parameters. The experimental data were obtained by testing the models in an arc-driven shock tube facility which produces a high enthalpy supersonic flow behind the traveling normal shock. With the models mounted in this shock-generated supersonic flow, the free-stream conditions with respect to the model were such that the equilibrium density ratio across the bow shock and the free-stream Mach number vary as $3.1 \leq k \leq 7.2$ and $2.1 \leq M_\infty \leq 3.54$, respectively. The stagnation enthalpy range for the tests (2,000-31,000 BTU/lb_m) allowed for free-stream dissociation and ionization levels of up to 88.0 per cent and 25.0 per cent, respectively. These free-stream conditions are not what is typically experienced in wind tunnels and free flight; thus, the handling of the data is somewhat different than usual in the type of quantities needed in the correlation procedure. It is demonstrated that the density ratio across the bow shock is the important parameter for correlating the nose region shock shapes since this produces agreement between the real gas data and perfect gas data. It is also demonstrated that detachment distance may be dependent on the level of free-stream dissociation while the nose region shock shape shows no dependence whatsoever on the degree of gas disscciation or ionization ahead of or behind the bow shock.

This Technical Documentary Report has been reviewed and is approved.

Philip P Antonatos

PHILIP P. ANTONATOS
Chief, Flight Mechanics Division
AF Flight Dynamics Laboratory

TABLE OF CONTENTS

LIST OF TABLES

ILLUSTRATIONS

ILLUSTRATIONS (Cont'd.)

LIST OF SYMBOLS

Symbol	
a_1	Speed of sound in the undisturbed gas ahead of traveling normal shock, ft/sec
A_1	Coefficient in equation describing shock wave profile in nose region, dimensionless
A_2	Coefficient in equation describing shock wave profile in cone region, dimensionless
b	Base diameter of 9 degree half-angle cone
C_D	Drag coefficient
d	Nose diameter of models
f	Focal length of mirror No. 2
h_T	Stagnation enthalpy, BTU/lb_m
k	Equilibrium density ratio across normal portion of bow shock = ρ_3/ρ_2
M_2	Flow Mach number of region 2 (equivalent to M_∞ for other types of data)
M_s	Traveling normal shock Mach number = V_s/a_1
n_1	Exponent in equation describing shock wave profile in nose region, dimensionless
n_2	Exponent in equation describing shock wave profile in cone region, dimensionless
P_1	Initial pressure in driven section of tube, mm Hg
q	Distance from mirror No. 2 to film
r	Radius of cross-section of shock wave
R_b	Nose radius of models
s	Distance from model to mirror No. 2
u_2	Flow velocity of gas in region 2, ft/sec

LIST OF SYMBOLS (Cont'd.)

Symbol	
V_s	Velocity of traveling normal shock, ft/sec
x	Coordinate along body axis, zero at wave apex
γ	Radio of specific heats
Δ	Distance from model to front edge of shock wave measured along body axis
μ_2	Mach angle for region 2, degrees

I. INTRODUCTION

In recent years there has been an increased interest in the shock shapes about blunt bodies since many aerodynamic quantities of interest depend on a knowledge of this shape. Many theoretical attempts have been made in this direction with only limited success especially in the nose region. The difficulty, as is generally known, is due to the existence of both subsonic and supersonic flow in this region. Fair success has been obtained with computer programs which use various methods to reach the sonic line, after which the method of characteristics is applied to develop the rest of the flow field about the body. Nevertheless, this approach is expensive in terms of computer time and gives only limited insight to the shock shape variation for a variety of initial conditions.

As a result, most of the published information on the nose region shock shapes has been experimental. The general procedure followed in most cases is to use an equation of the form indicated by blast wave theory in handling the data. Lin's[5] equation for the bow wave profile is

$$\frac{r}{d} = 0.80\, C_D^{1/4}\, (x/d)^{1/2} \quad , \tag{1}$$

where r and x are the bow wave coordinates, x taken along the axis of the body. The general form of this equation is

$$\frac{r}{d} = A(x/d)^n \quad , \tag{2}$$

where A and n are constants used in fitting the equation to certain regions of the shock wave. In the nose region, this equation indicates that the coordinate ratios form a straight line when plotted on a log-log scale, which is the case for most blunt bodies. The constants, A and n, are then correlated in some manner with the hope of writing a single expression for a range of initial conditions.

The parameter used most extensively for correlating A and n has been that of free-stream Mach number, but this does not seem to lead to any convenient expression for either constant. Recently, a new approach was taken in reference 2 where the stagnation enthalpy was the correlation parameter. In developing this correlation, experimental data and some computer results were used; the data at the high stagnation

Manuscript released by author, May 1964, for publication as an RTD Technical Documentary Report.

enthalpies were very limited. Based on this, it was felt that shock shapes observed in an arc-driven shock tube facility could possibly extend the work of reference 2 since this particular facility is capable of producing a wide range of stagnation enthalpies (1,700-61,000 BTU/lb$_m$). The one objection that might be raised to this technique is the limited free-stream Mach numbers of the test media (M_2 = 2.0-3.5), but as will be illustrated later, this does not affect the results when handled properly.

The present work forms one part of a more extensive hypersonic similitude study to establish which flow parameters are important when comparing various flow fields.

II. TEST FACILITY

The experimental data in this report were obtained in The Ohio State University arc-driven shock tube facility, which is capable of producing simulated flight velocities up to 50,000 ft/sec and simulated altitudes up to 200,000 ft, based on conditions in the stagnation region of a blunt model placed in the shock-generated flow. The energy used in driving this shock tube is supplied by a capacitor bank which has an energy capacity of 200,000 joules at its maximum voltage of 6000 (Fig. 1). The tube itself is conventional in the sense that both the driver and driven section have the same inside diameter--four inches. The driver section is separated from the driven section by a metal diaphragm prior to the start of a run. The driver is initially pressurized with helium to around 100 lb per square inch, while the driven section contains air to form the test media and is evacuated to some low pressure. The electrical energy stored in the capacitors is used to heat the helium to a high temperature and pressure thus causing the diaphragm to rupture. When the diaphragm breaks, a compression wave or shock wave is generated and moves into the low-pressure driven section, while an expansion wave propagates into the driver section in the opposite direction. A typical wave pattern is shown in Fig. 1a. Details on the performance of this facility have been reported previously[19,20] and will not be repeated here.

Two different tube configurations were used, one having a driven section 38 feet long; the second was 28 feet long. The longer driven section was coupled to the larger of two arc chambers, which has a volume of 0.116 cubic feet; the shorter tube was used in conjunction with the smaller arc chamber, which has a volume of 0.058 cubic feet. The configuration consisting of the shorter tube coupled to the small arc chamber supplied the higher shock speeds because of the higher pressures and temperatures produced in the driver gas. The shock Mach number range for the present tests was $5.9 \leq M_s \leq 25.5$, while the initial driven tube pressure ranged from 1.0 - 10.0 mm Hg.

III. TESTING TECHNIQUE

As indicated in Fig. 1, the driven section of the tube is terminated in a "dump tank", which serves two purposes:

1. To weaken the normal shock and prevent it from reflecting back up the tube to interfere with an experiment there.

2. To allow a model to be mounted in the free-jet supersonic flow of very high enthalpy.

These principles were utilized, with three different types of blunt bodies being mounted at the end of the driven section: A sphere; a hemisphere cylinder; and a 9 degree half-angle, spherically blunted cone. Actually, two 9 degree cone models of different bluntness ratios, nose diameter to base diameter of 0.250 and 0.660, were employed to facilitate the studies of the nose and cone regions.

A sample flow pattern is illustrated in Fig. 2. The normal shock moves past the model, followed by the shock-generated supersonic flow. The model itself must be mounted fairly close to the tube exit so as to minimize the effect of the disturbances which are created by the terminating tube and propagate out into the flow field at the Mach angle μ_2. Therefore, the useful testing core is cone-shaped with the height of the cone varying from 4-7 inches for the present tests. It is obvious from this consideration that the physical size of the models must be fairly small so that the flow pattern over the region of interest remains within the testing core.

A single-pass Z-type schlieren system with a capacitor-powered spark light source was used to photograph the shock pattern about the models. A schematic of the system is given in Fig. 3. Actually, two somewhat different configurations were employed throughout the testing program. The first configuration did not include the Kerr Cell; and, as a result, the proper time resolution was obtained by adjusting the spark light source until it had a 1-2 microsecond duration. This was accomplished by using a 6000 volt, 0.1 microfarad capacitor of low inductance.

The two ionization probes, ahead of the dump tank in Fig. 3, which detect the passage of the traveling normal shock, were used to measure shock velocity for later data reduction and to furnish a trigger pulse which initiated the light source. By properly adjusting the variable time delay between the second ionization probe and the light source, the flow pattern about the model was established prior to taking the data photograph.

A problem in flow of this nature which must be considered is that when the traveling normal shock first strikes the model, a portion of it is reflected and starts to form the bow shock. Since the process is initially an unsteady one, the newly formed bow shock tends to oscillate about its steady-state position until damping takes over and steady-state flow is obtained. Also, there is some finite time involved following the passage of the normal shock until the shocked gas reaches a state of equilibrium. Both of these processes are usually completed in about 10 microseconds from the time the normal shock first strikes the model. Following this interval, usable data may be obtained at any point prior

to the arrival of the contact region. The question of equilibrium of the shocked gas ahead of and behind the bow shock will be discussed further in the next section.

It must be noted at this point that the schlieren configuration without the Kerr Cell has certain limitations due to the radiant light from the high-temperature test gas. For this configuration, the film slide was removed prior to the start of a run and was not replaced until the run was completed. Depending on the particular test conditions, the slug of shock-generated test gas that flows over the model and past the dump tank window is from 20-100 microseconds in duration[21] Hence, since the test gas is at some elevated temperature, it gives off radiant light, part of which feeds through the optical portion of the system to the film. This means that the film is exposed to radiation from the test gas for 20-100 microseconds and to the spark light source for 1-2 microseconds. As a result, the increased gas radiation at the higher temperatures, corresponding to the higher shock Mach numbers, overrides the light source and blanks out the film. Using the standard knife edge ahead of the film, the upper limit of this system occurs at about a shock Mach number of 12.0 for an initial pressure of 1 mm Hg in the driven section. It was found that this limit could be extended to $M_s = 16.0$ for $P_1 = 1.0$ mm Hg by using a pinhole in place of the knife edge without significantly affecting the quality of the photographs. In doing this, all random radiation that originally might pass over the top of the knife edge is eliminated, and only that radiation which is being given off parallel will be passed on to the film.

To remove this limit and obtain data at higher shock velocities, $M_s > 16.0$, it was decided to reverse the schlieren configuration and use a high-speed optical shutter in front of the film such that the film was exposed to all radiation, test gas and light source, for some limited amount of time, around 2 microseconds. The Kerr Cell[22] satisfied the requirements for the optical shutter and was thus included in the system. Its main components consist of two crossed polaroids separated by a cell containing nitrobenzene in which two slanted high-voltage electrodes plates are immersed. In the closed position, the crossed polaroids prevent the light from passing through the cell. The open position is obtained by applying a pulse of 35,000 volts to the immersed electrodes, thus aligning the nitrobenzene molecules so that light rays passing through the first polaroid are rotated through 90 degrees and will then pass through the second polaroid. The passage of light continues as long as the high voltage remains on the electrodes; hence, the high-speed shutter action is obtained by controlling the duration of the high-voltage pulse.

One problem with the Kerr Cell exists in that it transmits only about 25 per cent of the light it receives, thus increasing the power requirements of the spark light source. The previously mentioned light source did not prove to be compatible with the Kerr Cell and it was necessary to obtain a commercially built source (manufactured by Unilectron of Boston, Massachusetts), which discharged 10 joules through an air gap in about one microsecond. Due to the one microsecond light

source duration and two microsecond Kerr Cell operation, the synchronization problem of the two was solved by firing the Kerr Cell directly from a pulse obtained upon the firing of the light source. With this type of synchronization, the operation of the system was the same as before, with the one time delay establishing the point where the photograph was to be taken. This configuration produced good results and eliminated all the test gas radiation problems.

One point of interest is that for sharp schlieren photographs, the lens equation must be applied in setting up the basic optical portion of the system. For the present arrangement, it can be stated as

$$\frac{1}{s} + \frac{1}{q} = \frac{1}{f} \quad , \tag{3}$$

where s is the distance from the model to mirror No. 2, q is the distance from mirror No. 2 to the film, and f is the focal length of mirror No. 2.

In reduction of the data, the photographs were enlarged and projected on a grid from which the coordinates of the shock wave were established. These coordinate values were non-dimensionalized by the nose diameter of the models before plotting them on a log-log scale. Since the non-dimensionalized coordinates for certain portions of the shock wave fall along a straight line, it was possible to write an expression for the shock in these regions in the form indicated earlier,

$$\frac{r}{d} = A(x/d)^n \quad , \tag{4}$$

and to determine the constants, A and n, for later use in correlating against one of the flow parameters. Several typical data pictures are shown in Fig. 4. It is noted that the deviation in the curvature of the shock wave towards the edge of the photograph indicates the limit of the useful test core.

IV. DISCUSSION OF DATA

Referring again to Fig. 2, it is noted that the properties of region 2 form the free-stream properties with respect to the model, and that M_2 corresponds to M_∞ for other types of data, wind tunnels, etc. When analyzing the present type of data, the questions that must first be answered are: (1) is region 2 of sufficient duration to obtain data, (2) what is the equilibrium state of the gas in region 2; and (3) how do

the flow properties in this region vary with the different test conditions?

The first question was answered in the preceding section. The duration of region 2 is from 20-100 microseconds over the present range of conditions, and since only 10 microseconds is needed to establish steady state flow, there is still adequate time to obtain data.

The second question is somewhat more involved and can be answered only after an extensive study of the facility. Based on such a study, Fig. 5 shows a typical photomultiplier trace of the time history of radiation from the gas in region 2. This trace was obtained by positioning the photomultiplier such that observations were made through a collimated slit system of the free-jet exhausting into the dump tank. The actual observation point was again taken as near as possible to the driven tube exit to eliminate expansion effects. The trace shows the non-equilibrium overshoot behind the normal shock, followed by a region of constant radiation, which indicates that the gas was in chemical and thermal equilibrium. Following the region of constant radiation, there is another increase which signifies the passage of the contact region and the end of the useful test period. Since the schlieren photograph was timed to be taken in the region of constant radiation, the gas ahead of the bow wave should have been in chemical and thermal equilibrium.

The last question pertaining to the flow properties of region 2 has been answered by references 12, 13, 14, 15, and 16. The Mach number of the flow (Fig. 7) was calculated using the equilibrium speed of sound. It is noted that the variation in the Mach number is rather limited in that it varies from 2.0 - 3.5 for $6 \leq M_s \leq 30$, and, as a result, it may be considered as nearly constant. The variation in the equilibrium density ratio across the bow shock of the model (Fig. 8) goes from 2.1-7.3 for $6 \leq M_s \leq 30$ and remains fairly constant for $M_s \geq 17.0$. The significance of this fact will become obvious when the shock wave constants are discussed. Figure 9 shows how the per cent of gas dissociation and ionization in region 2 varies with shock Mach number. Since the test conditions for the upper limit of the data obtained were $M_s = 25.5$ and $P_1 = 1.0$ mm Hg., the peak free-stream dissociation was 92.0 per cent and only a trace of ionization was experienced. It will be pointed out later that the shock wave dependence on these parameters is negligible.

It should probably be noted at this point that references 1, 2, 4, 9, 10, 11, 18, and 23 are used only as sources of experimental data. These data are used for comparison purposes and to help formulate the shock wave correlation presented below.

A. DETACHMENT DISTANCE

One of the first quantities considered in analyzing the data was that of detachment distance and how it compared with data taken in other

facilities, perfect gas data. Since the gas being dealt with is a real gas, the ratio of specific heats behind the bow shock, γ, is something less than 1.4. The dependence of detachment distance on γ is shown in Fig. 10. It is noted that the dependence is only slight; therefore the $\gamma = 1.0$ curve was used, along with Serbin's[6] theory and the theory of Li and Geiger,[7] to compare with the experimental data (Fig. 11). In considering this plot, one observes that the real gas data compares favorably with theory and the perfect gas data for $k \leq 5.0$, but above this point there is an increasing separation in the results, with the perfect gas data and theory falling below the real gas data.

The reason for this is not yet apparent. It might be rash to think that there should be any agreement, but since there is agreement at the lower density ratios, it seems reasonable that it should continue at the higher. One possibility for the deviation could be a non-equilibrium effect behind the bow shock, but by considering Fig. 6 (taken from reference 17), this theory is more or less eliminated since it indicates the region to be in non-equilibrium for all points for which $M_s \leq 17.0$. This means that there are only a few data points around $k = 7.0$ which are in equilibrium, and the remaining points are in non-equilibrium. Since non-equilibrium effects cause the detachment distance to increase over the equilibrium case, this does not seem to be the answer; there is agreement between the real and perfect gas points at the lower values of density ratio. Therefore, the indication is that Fig. 6 is only an extreme upper limit on the equilibrium distance required behind the bow shock. Another possibility might be a Reynolds number effect, but this is quickly eliminated since the free-stream, region 2, Reynolds number is so large, 43,000-95,000/in., over the present range. The only other possibility is that the detachment distance is a function of the free-stream dissociation level, for which there is no conclusive indication. Further investigations are being carried out at The Ohio State University, and until they are completed, it is impossible to determine the reason for the deviation between the real gas and perfect gas data. The variation of detachment distance with stagnation enthalpy is shown in Fig. 12.

B. SHOCK SHAPE

As for the dependence of the shock wave profile on real gas effects, Fig. 13 shows two wave profiles at approximately the same free-stream Mach number, one perfect gas and one real gas taken from the present data. The author realizes that one does not normally think of real gas effects occurring at such a low Mach number as indicated on the plot; but because of the low free-stream Mach number of the shock tube flow, it was necessary to make the comparison in this range. The reason for presenting the plot is to demonstrate that the shock wave profile depends on something other than free-stream Mach number, since it is noted that the real gas profile lies closer to the body than the perfect gas profile. The cause of the deviation in the two profiles is that the density ratio across the normal portion of the bow shock is higher in the real gas case than in the corresponding perfect gas case, thus causing the shock wave to move in toward the body.

This portion of the investigation was divided into two sections, one considering only the nose region profile using sphere, hemisphere cylinder, and a 9 degree half-angle, spherically blunted cone; and the other considering the profile over the cone region of the 9 degree blunted cone. The shock coordinates were treated as indicated earlier, with A_1 and n_1 being the wave constants for the nose region and A_2 and n_2 being the wave constants for the cone region.

In searching for a convenient correlation parameter for the A_1 and n_1 constants, they were first plotted as functions of stagnation enthalpy, since this was the parameter indicated in reference 2 and was the flow parameter of greatest variation for the shock tube facility employed (Fig. 15). In considering this plot and comparing with the data of reference 2, it is noted that the deviation between the two sets of A_1 and n_1 values is such that they both have the same trend, the real gas data being displaced some finite amount. It must be remembered that the real gas free-stream Mach number is about 3.0 while that for the other data is $2.0 \leq M_\infty \leq 19.25$. With this in mind, it was concluded that the deviation was a Mach number effect; and, as a result, the quantities $A_1 - 2.3/M_2^2$ and $n_1 - 1/2M_2^2$ were used in order to bring the two sets of data together (Fig. 16). This still did not produce a convenient correlation for the A_1 constant; nevertheless, it did indicate the correct expression for n_1, with the quantity $n_1 - 1/2M_2^2$ remaining relatively constant throughout the enthalpy range.

The wave constants were finally plotted against the equilibrium density ratio across the normal portion of the bow shock, using the quantities $A_1 - 1/M_2^2$ and $n_1 - 1/2M_2^2$ to coordinate all the data (Fig. 17). This is in accordance with the handling of detachment distance and seems to be the correct correlation parameter since the real gas values of A_1 show good agreement with values taken from wind tunnel tests for $k \leq 6.0$. The deviation in the real gas values of A_1 for $k > 6.0$ can be explained, based on the characteristics of the shock tube flow, in that the density ratio has stabilized at some value while the flow Mach number, M_2, is still increasing slightly. Since all the nose region profile data above a shock Mach number of 16.2 was taken at an initial pressure of 1-2 mm Hg in the driven section, the equilibrium density ratio stabilizes at about $k = 7.0$ for $M_s \geq 17.0$, while the flow Mach number keeps increasing until $M_s = 22.0$. This means that with the shock shape being a function of the density ratio, A_1 and n_1 should be relatively constant for $M_s \geq 17.0$. Considering the present high enthalpy data in Fig. 15, it is noted that this is exactly the situation. Hence, with a constant shock shape, the decreasing value of $1/M_2^2$ causes the deviation observed in Fig. 17. The significance of A_1 and n_1 being constant above $M_s = 17.0$ is also noted by the fact that the nose region shock shape shows no dependence on the gas dissociation or ionization level ahead of or behind the bow shock, since these quantities increase in magnitude with increasing stagnation enthalpy.

The $n_1 - 1/2M_2^2$ values in Fig. 17 show some variation, especially at the low values of density ratio. The reason for this is not obvious, but it is probably due simply to experimental error, since n_1 is the slope of a straight line on a log-log plot. Nevertheless, based mainly

on the present data, the indicated empirical expression for n_1 would be

$$n_1 = 0.445 + \frac{1}{2M_2^2} \quad , \qquad \text{for } 2 \leq k \leq 15 \quad . \qquad (5)$$

Also, the indicated empirical expressions for A_1 are

$$A_1 = 1.5 - 0.0784k + \frac{1}{M_2^2} \quad , \qquad \text{for } 2 \leq k \leq 6 \quad , \qquad (6)$$

and

$$A_1 = 1.13 - 0.0167k + \frac{1}{M_2^2} \quad , \qquad \text{for } 6 \leq k \leq 15 \quad . \qquad (7)$$

The complete shock wave shape over the 9 degree blunted cone can be expressed as two straight lines on a log-log scale as shown in Fig. 14. The constants for the cone region are determined in the usual manner, after which they are plotted against the previously established correlation parameter of density ratio (Fig. 18). It is observed that the scatter in the $n_2 - 1/2M_2^2$ value is much greater than for the equivalent quantity in the nose region; and that the trend for $n_2 - 1/2M_2^2$ is a decrease, with increasing k, while $n_1 - 1/2M_2^2$ remains constant. There are practically no wind tunnel data available for 9 degree blunted cones in the present range of density ratio; hence, it is difficult to draw any conclusions as to the correlation of this data. Also, there does not seem to be any convenient expression for the shock-wave constant of A_2 as there was in the case of the nose region profile. If the scatter in $n_2 - 1/2M_2^2$ can be neglected, a straight line could be drawn through the points; nevertheless, if any of the cone region data are to be put to use, the values of A_2 and n_2 should undoubtedly be obtained directly from Fig. 18.

V. CONCLUSIONS

The real gas detachment distance data show agreement with theory and with perfect gas data at the low equilibrium density ratios, while it disagrees at the high ratios. The reason for this is not readily apparent, but it could possibly be an effect due to the free-stream level of gas dissociation. It was found that the real gas as well as the perfect gas shock wave profile could be represented by an equation of the form

$$r/d = A\left(\frac{x}{d}\right)^{n} \quad . \tag{8}$$

The constants in this equation, A, and n_1, for the nose region portion of the shock profile do not correlate against the parameter of stagnation enthalpy indicated in reference 2, but they do correlate very well against the equilibrium density ratio across the normal portion of the bow shock. As was demonstrated, the nose region shock-wave profile for the real gas situation does not depend in any manner on the level of gas dissociation or ionization ahead of or behind the bow shock. The shock wave constant of A_1 becomes strictly a function of density ratio for $M_\infty \geq 15.0$, while n_1 assumes the constant value of 0.445; thus the shock profile in the nose region of a body in flight becomes solely a function of density ratio beyond the above-stated free-stream Mach number limit. The cone region shock wave constants show a somewhat different variation from that of the nose region in that $n_2 - 1/2M_2^2$ decreases with increasing equilibrium density ratio, while $n_1 - 1/2M_2^2$ remains constant. No convenient expressions can be written for the cone region shock wave constants; also, no statement can be made as to whether or not the correlation has general application until further perfect gas data are obtained for comparison.

REFERENCES

1. Lees, L., and Kubota, T., "Inviscid Hypersonic Flow Over Blunt-Nosed Slender Bodies," J. Aero. Sci., Vol. 24, February, 1957, pp 195-202.

2. Seiff, A., and Whiting, E. E., "A Correlation Study of the Bow-Wave Profiles of Blunt Bodies," NASA TN D-1148, February, 1962.

3. Lobb, K. R., "Experimental Measurement of Shock Detachment Distance on Spheres Fired in Air at Hypervelocities," Naval Ordnance Laboratory, April, 1962.

4. Baer, A. L., 'Pressure Distributions on a Hemisphere-Cylinder at Supersonic and Hypersonic Mach Numbers," AEDC-TN-61-96, August, 1961.

5. Lin, S. C., "Cylindrical Shock Waves Produced by Instantaneous Energy Release," J. Appl. Phys., Vol. 25, No. 1, January, 1954 pp 54-57.

6. Serbin, H., "Supersonic Flow Around Blunt Bodies," J. Aero. Sci., Vol. 25, January, 1958, pp 58-59.

7. Li, T. Y., and Geiger, R. E., "Stagnation Point of a Blunt Body in Hypersonic Flow," J. Aero. Sci., Vol. 24, January, 1957, pp 25-32.

8. Van Dyke, M. D., and Gordon, H. D., "Supersonic Flow Past a Family of Blunt Axisymmetric Bodies," NASA Technical Report R-1, 1959.

9. Oliver, R. E., "An Experimental Investigation of Flow Over Simple Blunt Bodies at a Nominal Mach Number of 5.8," J. Aero. Sci., Vol. 23, February, 1956, pp 177-179.

10. Vas, I. E.; Bogdonoff, S. M.; and Hammitt, A. G., "An Experimental Investigation of the Flow over Simple Two-Dimensional and Axial Symmetric Bodies at Hypersonic Speeds," WADC TN-57-246, AD 130826. Princeton University Report No. 382, June, 1957.

11. Love, E. S., "A Re-examination of the Use of Simple Concepts for Predicting the Shape and Location of Detached Shock Waves," NACA TN-4170, 1957.

12. Feldman, S., "Hypersonic Gas Dynamic Charts for Equilibrium Air," Avco Research Laboratory, Avco Manufacturing Corporation, Everett, Massachusetts, January, 1957.

13. Ziemer, R. W., "Extended Hypervelocity Gas Dynamic Charts for Equilibrium Air," STL/TR-60-0000-09093, Space Technology Laboratories, Inc., April, 1960.

14. Hansen, C. F., "Approximations for the Thermodynamic and Transport Properties of High Temperature Air," NASA TR-R-50, 1959.

15. Scala, S. M., "The Hypersonic Environment Heat Transfer in Multicomponent Gases," General Electric Report R62SD987, Space Sciences Laboratory, December, 1962.

16. Gilmore, F. R., "Equilibrium Composition and Thermodynamic Properties of Air to 24,000°K," Rand Corporation RM-1543, August, 1955.

17. Rose, P. H., and Stankevics, J. O., "Stagnation Point Heat Transfer Measurements in Partially Ionized Air," Institute of Aerospace Sciences, 31st Annual Meeting, No. 63-61, January, 1963.

18. The Ohio State University Aerodynamic Laboratory. Private communications with G. M. Gregorek.

19. Lee, J. D., and Nerem, R. M., "Theory and Performance of a Shock Tube Having an Arc-Heated Driver," The Ohio State University Aerodynamic Laboratory Report No. 1021-18, June, 1962.

20. Caldecott, R. L.; Lee, J. D.; and Nerem, R. M., "Development and Application of an Arc-Driven Hypervelocity Shock Tube," Institute of Technology, April 1-3, 1963.

21. Graber, B. C., and Nerem, R. M., "Test Duration Measurements in an Arc-Driven Hypervelocity Shock Tube," The Ohio State University Aerodynamic Laboratory, No. 1573-2.

22. Zarem, A. M.; Marshall, F. R.; and Hauser, S. M., "Millimicrosecond Kerr Cell Camera Shutter," Review of Scientific Instruments, Vol. 29, No. 11, November, 1958, pp 1041-1044.

23. Nagamatsu, H. T.; Geiger, R. E.; and Sheer, Jr., R. E., "Real Gas Effects in Flow over Blunt Bodies at Hypersonic Speeds," General Electric Report 59-RL-2177, Research Laboratory, Schenectady, New York, February, 1959.

TABLE I. DETACHMENT DISTANCE DATA

RUN	k	$h_m \times 10^{-3}$ BTU/lb$_m$	Δ/R_b	M_s	P_1 mm Hg
		SPHERE			
1658	4.6	3.62	0.191	8.8	3.0
1659	4.15	2.77	0.219	7.8	5.0
2332	5.81	8.30	0.158	13.2	2.0
2333	6.13	10.50	0.151	14.8	2.0
2335	6.74	13.00	0.145	16.6	2.0
2336	7.22	19.10	0.137	19.9	2.0
2345	7.00	22.90	0.126	21.8	2.0
2354	6.81	27.70	0.142	24.1	1.0
2359	6.83	26.35	0.129	23.5	1.5
2360	7.10	21.70	0.144	21.2	2.0
2362	4.87	5.90	0.183	11.2	5.0
2376	5.50	8.30	0.163	13.2	5.0
2378	6.05	10.92	0.157	15.1	5.0
2379	4.20	3.05	0.222	8.1	10.0
		HEMISPHERE CYLINDER			
1606	6.04	8.70	0.143	13.5	1.0
1611	4.84	4.90	0.179	10.2	1.0
1612	5.18	5.80	0.166	11.1	1.0
1615	5.72	7.40	0.156	12.5	1.0
1627	4.7	4.50	0.176	9.8	2.0
1635	4.57	3.30	0.192	8.4	2.0
2339	6.82	14.00	0.138	17.1	2.0
2341	6.85	15.90	0.144	18.2	2.0
2351	6.67	12.55	0.141	16.2	2.0
2352	6.6	12.10	0.147	15.9	2.0
2355	6.8	31.00	0.140	25.5	1.0
2380	5.92	8.70	0.154	13.5	2.0
2384	5.1	6.70	0.174	11.9	5.0

TABLE I. (continued)

RUN	k	$h_T \times 10^{-3}$ BTU/lb_m	Δ/R_b	M_s	P_1 mm Hg	d/b
		SPHERICAL NOSED CONE				
1692	6.31	9.80	0.139	14.3	1.0	0.660
1693	6.52	10.80	0.140	15.0	1.0	0.660
1695	6.81	12.25	0.142	16.0	1.0	0.660
1698	5.03	5.70	0.170	11.0	2.0	0.660
1699	4.92	5.40	0.168	10.7	2.0	0.660
1700	4.67	4.40	0.187	9.7	2.0	0.660
1702	4.31	3.10	0.207	8.2	5.0	0.660
1703	5.64	7.20	0.151	12.3	1.0	0.660
2342	6.94	17.40	0.137	19.0	2.0	0.660
2343	7.06	18.30	0.140	19.5	2.0	0.660
2347	7.24	19.90	0.132	20.3	2.0	0.660
2348	6.96	24.05	0.143	22.4	1.5	0.660
2357	6.80	29.55	0.142	24.9	1.0	0.660
2385	4.45	3.75	0.190	9.0	10.0	0.660
2387	6.58	11.95	0.149	17.8	2.0	0.660

TABLE II. SHOCK WAVE PROFILE DATA

RUN	M_2	k	$h_T \times 10^{-3}$ BTU/lb$_m$	A_1	n_1	M_s	P_1 mm Hg
			SPHERE				
1654	2.77	5.66	7.55	1.170	0.495	12.7	2.0
1656	2.74	5.21	6.47	1.210	0.501	11.8	3.0
1658	2.52	4.60	3.62	1.280	0.541	8.8	3.0
1659	2.30	4.15	2.77	1.350	0.538	7.8	5.0
2128	2.13	3.60	2.11	1.440	0.551	6.8	10.0
2129	2.04	3.10	1.59	1.510	0.560	5.9	10.0
2131	2.28	4.10	2.87	1.365	0.545	7.9	10.0
2198	3.05	6.27	12.50	1.140	0.505	16.2	5.0
2332	2.82	5.81	8.30	1.185	0.513	13.2	2.0
2333	3.00	6.31	10.50	1.160	0.508	14.8	2.0
2336	3.44	7.22	19.10	1.135	0.488	19.9	2.0
2344	3.49	7.19	20.70	1.120	0.494	20.7	2.0
2346	3.53	7.00	22.90	1.125	0.488	21.8	2.0
2350	3.55	6.97	23.80	1.120	0.489	22.3	1.5
2353	3.49	6.77	29.55	1.140	0.491	24.9	1.5
2354	3.54	6.81	27.70	1.130	0.486	24.1	1.0
2359	3.54	6.83	26.35	1.135	0.486	23.5	1.5
2360	3.51	7.10	21.70	1.115	0.486	21.2	2.0
2362	2.75	4.87	5.90	1.235	0.512	11.2	5.0
2379	2.32	4.20	3.05	1.370	0.546	8.1	10.0
Supersonic Blowdown Tunnel	2.02	2.70	0.128	1.550	0.567		
			HEMISPHERE CYLINDER				
1605	2.94	6.20	9.42	1.140	0.493	14.0	1.0
1612	2.81	5.18	5.15	1.205	0.507	11.1	1.0
1615	2.78	5.72	7.30	1.190	0.503	12.5	1.0
1620	3.05	6.52	10.69	1.135	0.494	15.0	1.0
1627	2.72	4.70	4.51	1.245	0.525	9.8	2.0
2339	3.22	6.82	14.00	1.130	0.501	17.1	2.0
2341	3.32	6.85	15.90	1.120	0.491	18.2	2.0
2349	3.54	6.89	25.10	1.115	0.484	22.9	1.5
2351	3.13	6.67	12.55	1.150	0.492	16.2	2.0
2355	3.46	6.80	31.00	1.120	0.487	25.5	1.0
2356	3.48	6.80	29.55	1.125	0.485	24.9	1.0
2380	2.86	5.92	8.70	1.185	0.506	13.5	2.0
2384	2.72	5.10	6.70	1.220	0.514	11.9	5.0

TABLE II - (continued)

RUN	M_2	k	$h_T \times 10^{-3}$ BTU/lb$_m$	A_1	n_1	M_s	P_1 mm Hg	d/b
			SPHERICAL NOSED CONE					
1689	2.77	5.40	6.42	1.190	0.510	11.7	1.0	0.660
1690	2.87	6.04	8.48	1.150	0.505	13.4	1.0	0.660
1695	3.15	6.81	12.13	1.150	0.504	16.0	1.0	0.660
1699	2.80	4.92	5.42	1.220	0.507	10.7	2.0	0.660
1701	2.57	4.66	3.86	1.300	0.535	9.1	3.0	0.660
1702	2.37	4.31	3.14	1.350	0.536	8.2	5.0	0.660
1703	2.77	5.64	7.06	1.175	0.506	12.3	1.0	0.660
2342	3.37	6.94	17.40	1.130	0.496	19.0	2.0	0.660
2343	3.41	7.06	18.30	1.125	0.484	19.5	2.0	0.660
2347	3.46	7.24	19.90	1.115	0.483	20.3	2.0	0.660
2348	3.55	6.96	24.05	1.130	0.492	22.4	1.5	0.660
2357	3.48	6.80	29.55	1.130	0.491	24.9	1.0	0.660
2358	3.46	6.80	31.00	1.125	0.492	25.5	1.0	0.660
2387	3.20	6.47	15.20	1.135	0.495	17.8	2.0	0.660
				A_2	n_2			
2113	2.79	5.10	5.90	1.170	0.635	11.2	2.0	0.660
2114	2.66	4.60	4.60	1.230	0.662	9.9	5.0	0.660
2116	2.75	4.80	5.60	1.200	0.654	10.9	5.0	0.660
2117	2.75	4.91	6.00	1.195	0.643	11.3	5.0	0.660
2121	2.64	4.55	4.30	1.230	0.689	9.6	10.0	0.250
2122	2.37	4.28	3.30	1.305	0.685	8.4	10.0	0.250
2123	2.30	4.15	3.00	1.330	0.704	8.0	10.0	0.250
2124	2.24	3.97	2.80	1.375	0.707	7.6	10.0	0.250
2126	2.16	3.75	2.20	1.410	0.734	7.1	10.0	0.250
2132	2.28	4.07	2.90	1.350	0.722	7.9	10.0	0.250
2133	2.67	4.65	4.85	1.220	0.682	10.2	10.0	0.250
2363	2.70	4.82	6.20	1.220	0.676	11.5	10.0	0.250
2364	2.70	5.00	6.80	1.200	0.676	12.0	10.0	0.250
2366	2.75	5.49	8.55	1.180	0.669	13.4	8.4	0.250
2367	2.71	5.30	7.80	1.190	0.646	12.8	8.4	0.250
2368	2.82	5.70	9.65	1.175	0.662	14.2	8.4	0.250
2369	2.92	5.96	11.10	1.150	0.675	15.2	8.4	0.250
2370	3.01	6.20	12.00	1.135	0.654	15.8	5.0	0.660
2372	2.99	6.18	11.65	1.135	0.646	15.6	5.0	0.660
2373	3.15	6.40	14.20	1.125	0.631	17.2	5.0	0.660
2374	3.30	6.64	16.60	1.115	0.610	18.6	4.0	0.660
2375	3.40	7.00	19.10	1.105	0.604	19.9	3.0	0.660
2377	3.35	6.80	17.55	1.110	0.612	19.1	3.0	0.660

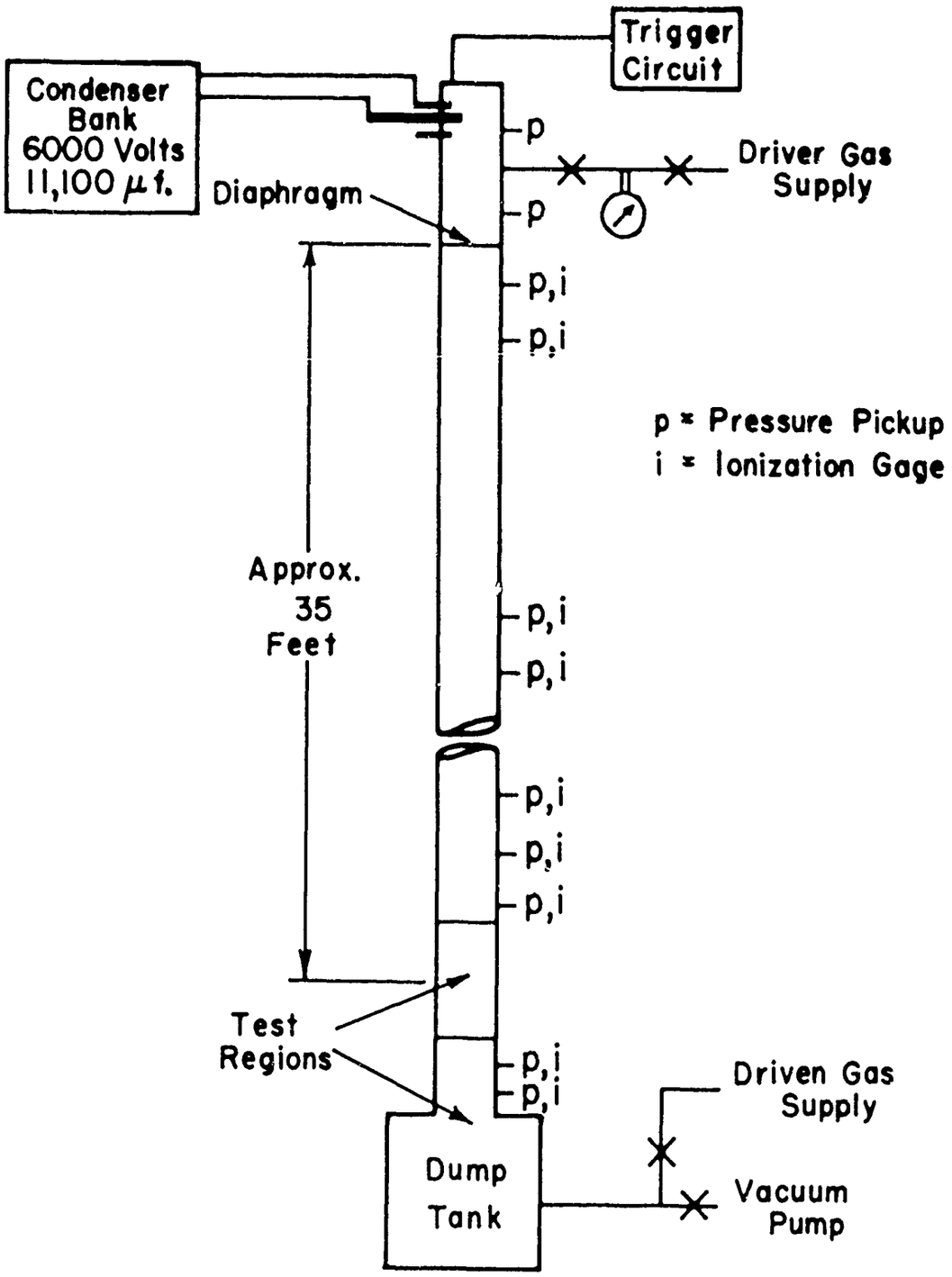

FIGURE 1 — LAYOUT OF SHOCK TUBE SYSTEM

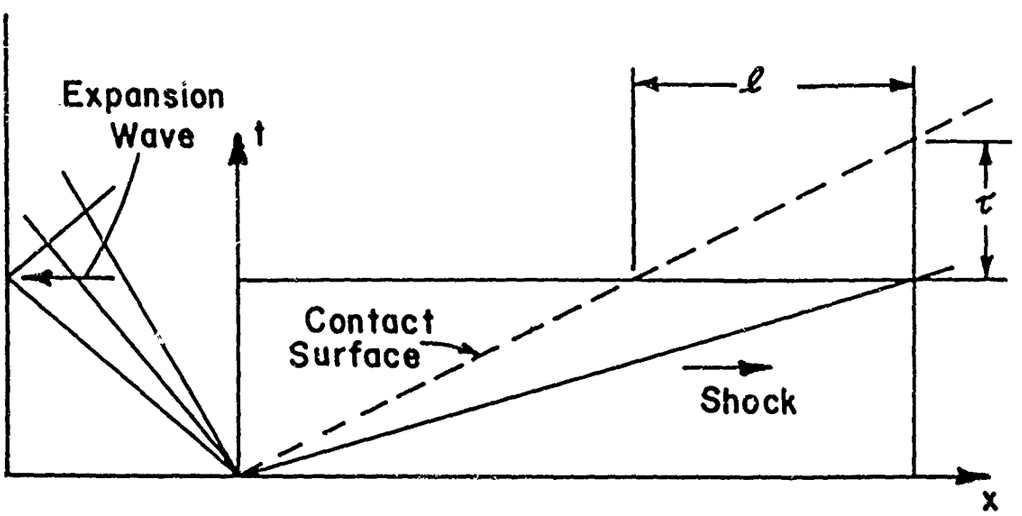

FIGURE 1a.— FLOW PATTERN IN CONSTANT AREA SHOCK TUBE

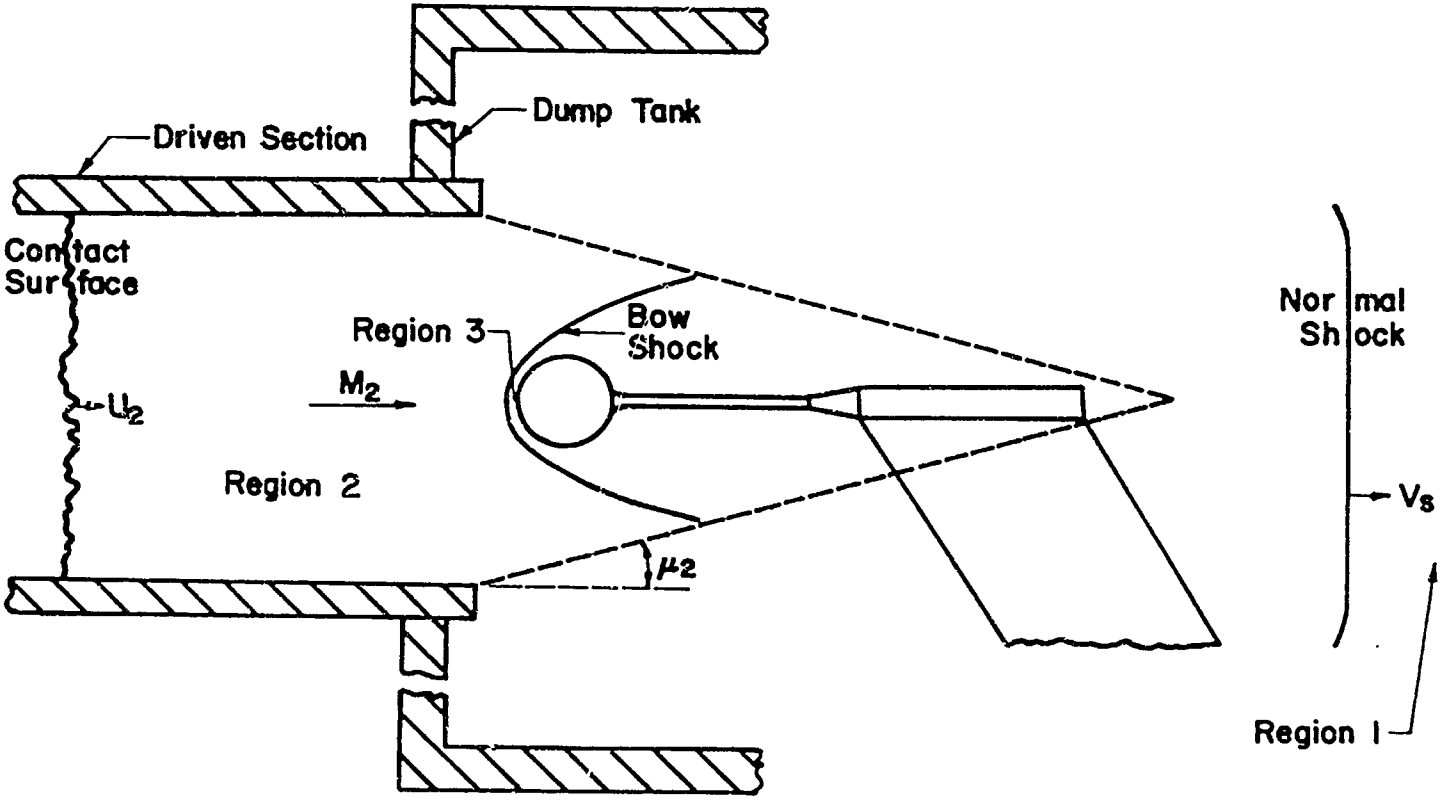

FIGURE 2 - FLOW PATTERN ABOUT FIXED MODEL

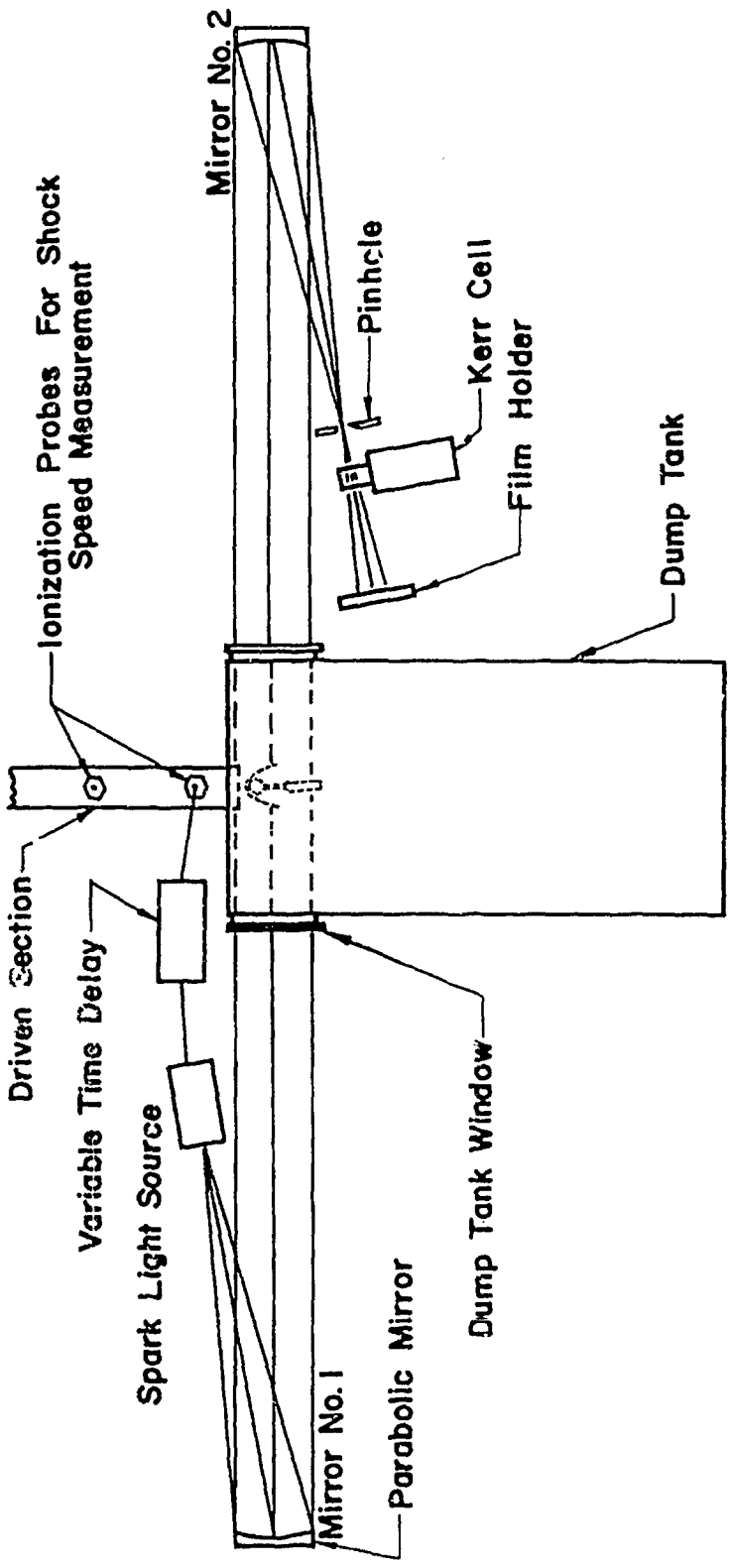

FIGURE 3 - SCHEMATIC OF SCHLIEREN SYSTEM

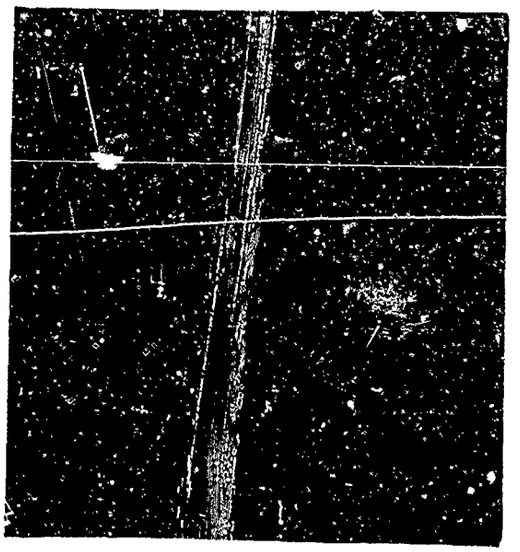

$k = 4.87 \quad h_T = 5{,}900 \text{ BTU/lb}_m$

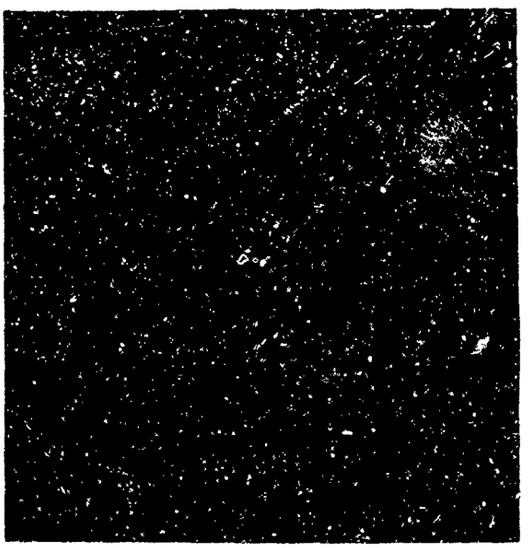

$k = 7.10 \quad h_T = 21{,}700 \text{ BTU/lb}_m$

FIGURE 4 — TYPICAL SCHLIEREN PHOTOGRAPHS

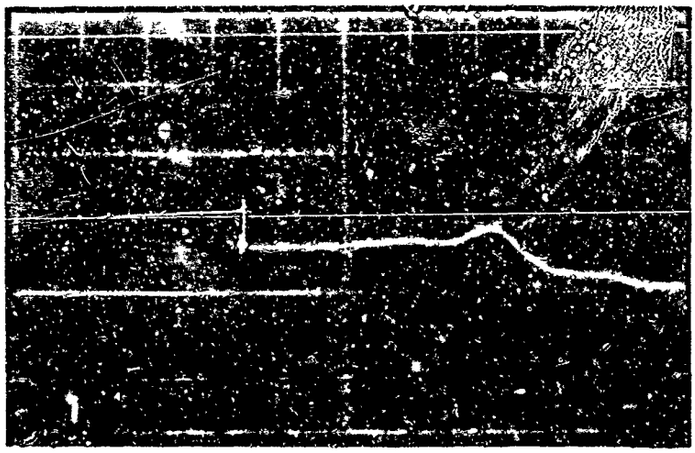

P_1 = 1.0 mmHg M_S = 23 5

Time Scale : $5\mu sec/cm$

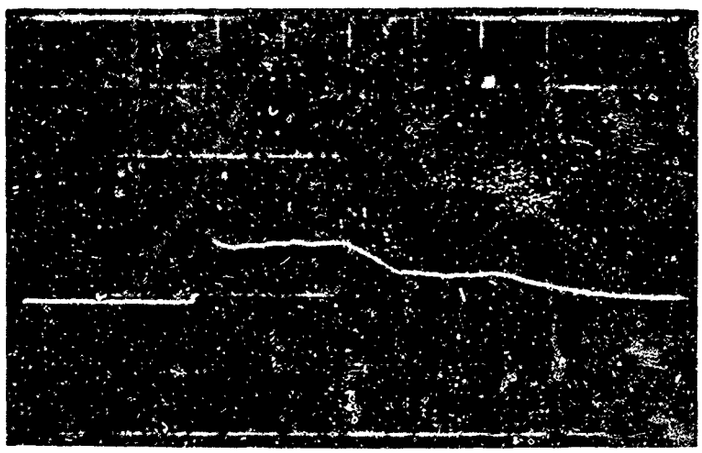

P_1 = 1 0 mmHg M_S = 25

Time Scale: $5\mu sec/cm$

FIGURE 5 — TYPICAL VARIATION OF RADIATION INTENSITY BEHIND TRAVELING NORMAL SHOCK (3000-5000Å)

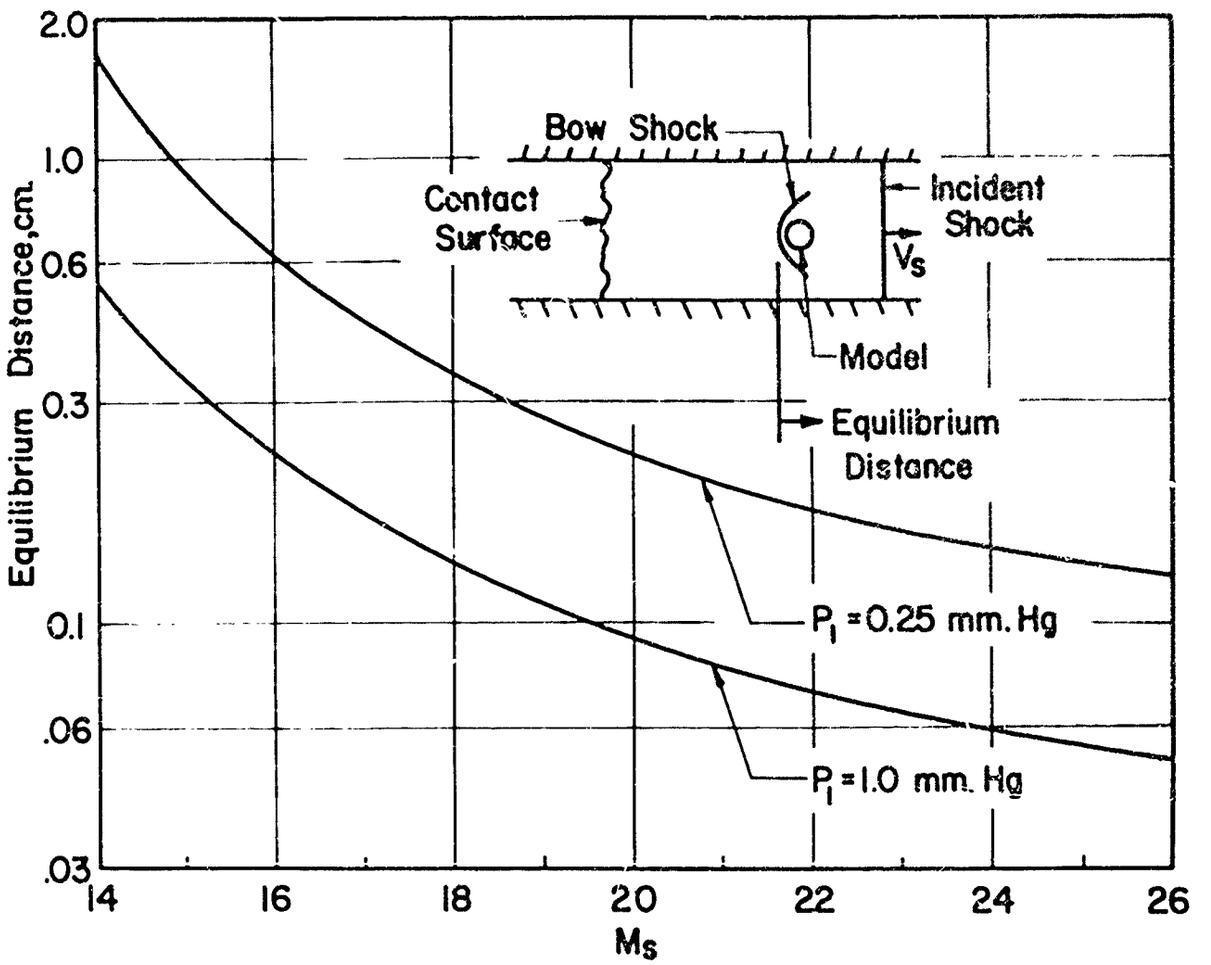

FIGURE 6- DISTANCE BEHIND BOW SHOCK TO ESTABLISH EQUILIBRIUM VERSUS SHOCK MACH NUMBER (REF. 17)

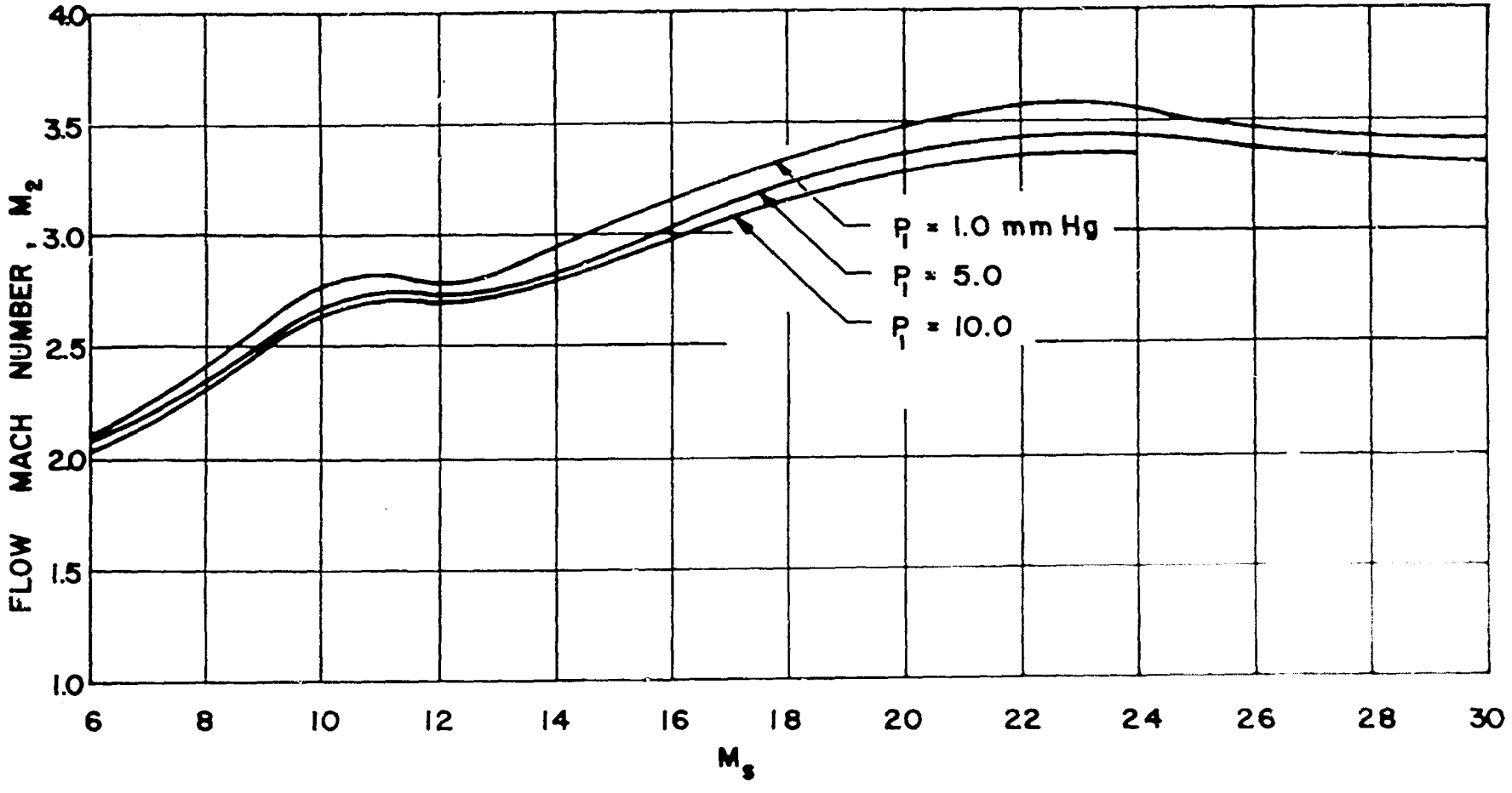

FIGURE 7 — MACH NUMBER OF SHOCK GENERATED SUPERSONIC FLOW VERSUS SHOCK MACH NUMBER

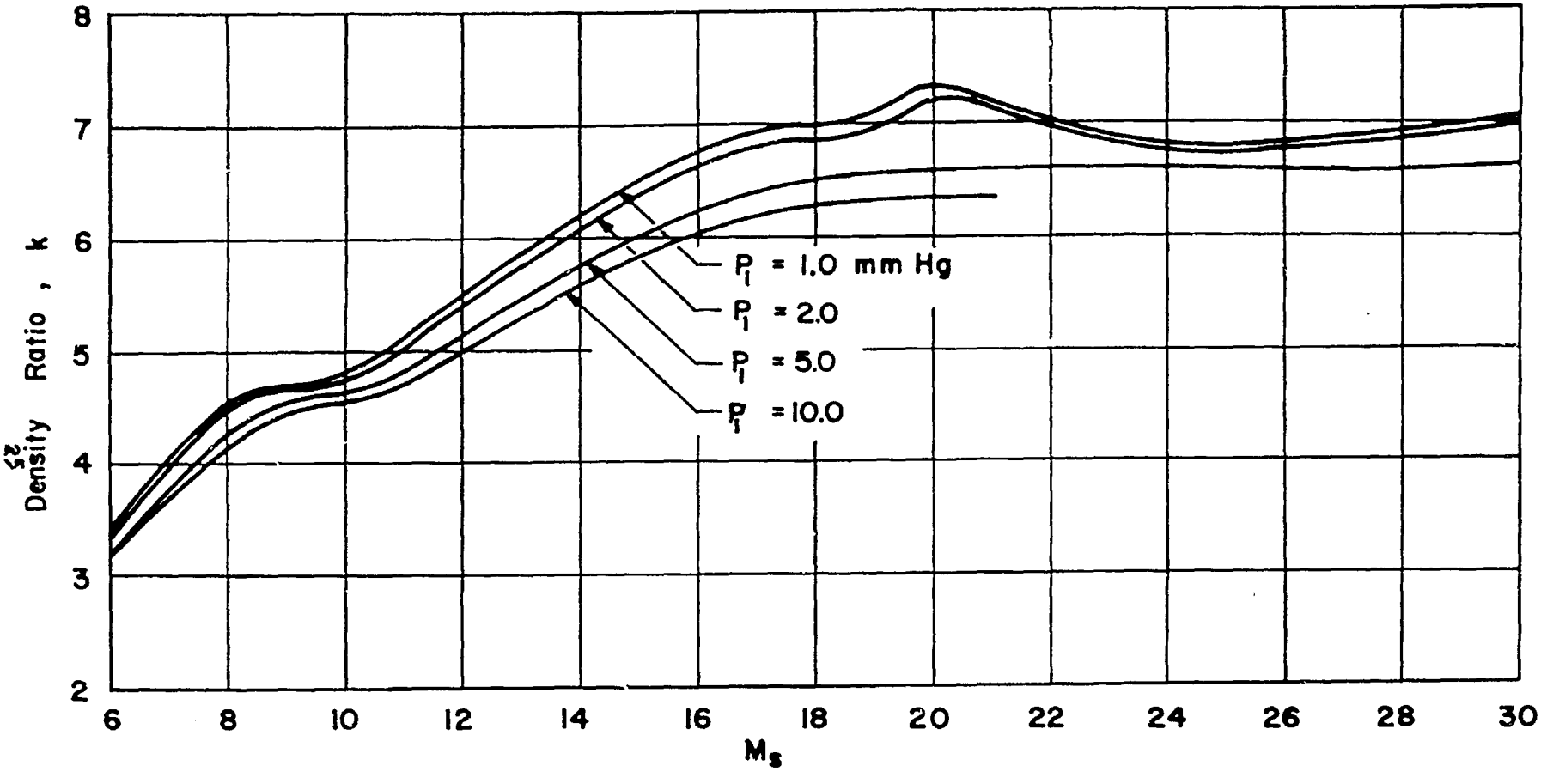

FIGURE 8 — EQUILIBRIUM DENSITY RATIO ACROSS NORMAL PORTION OF BOW SHOCK VERSUS SHOCK MACH NUMBER

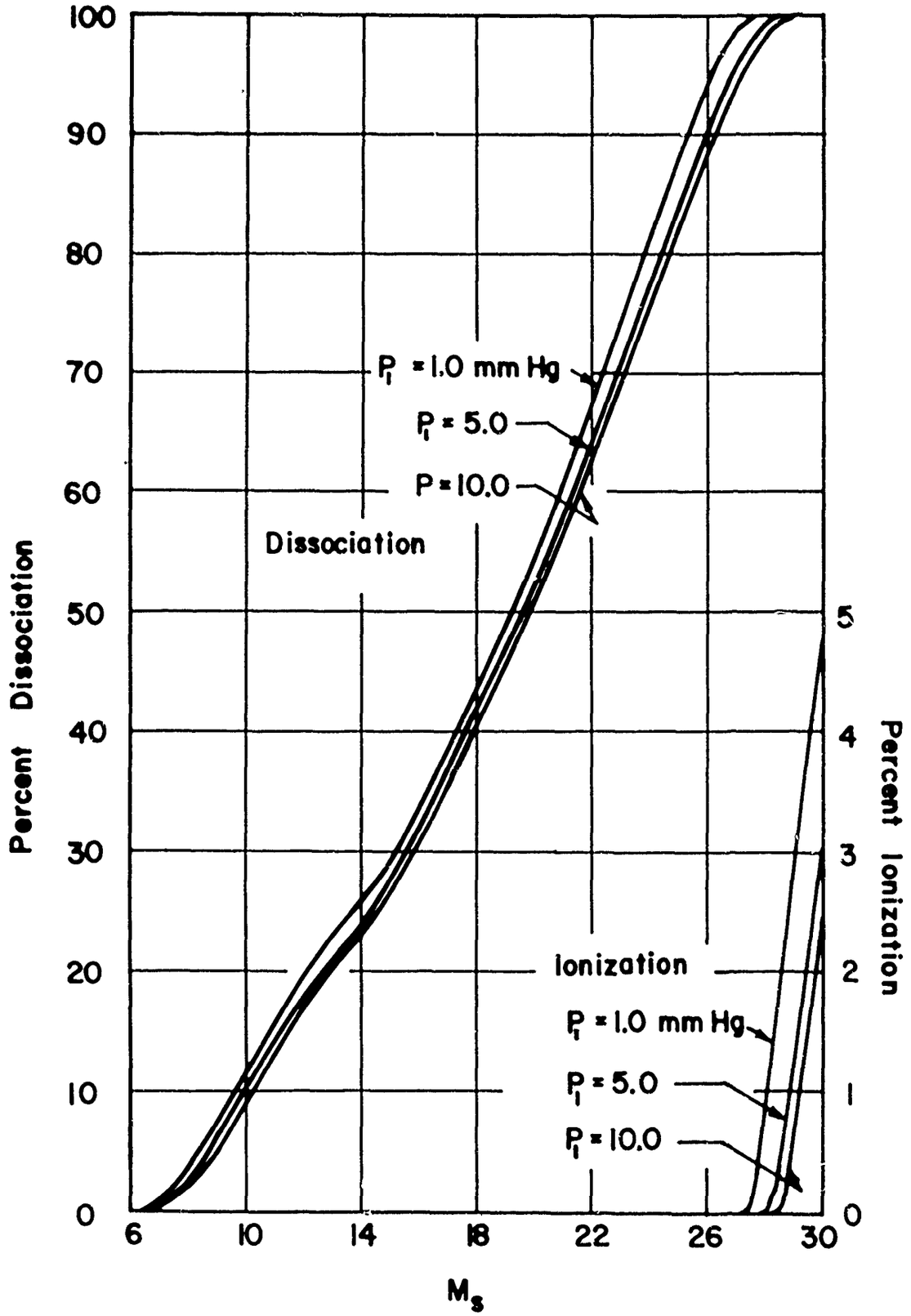

FIGURE 9 – PERCENT OF GAS DISSOCIATION AND IONIZATION IN REGION 2 vs. SHOCK MACH NUMBER

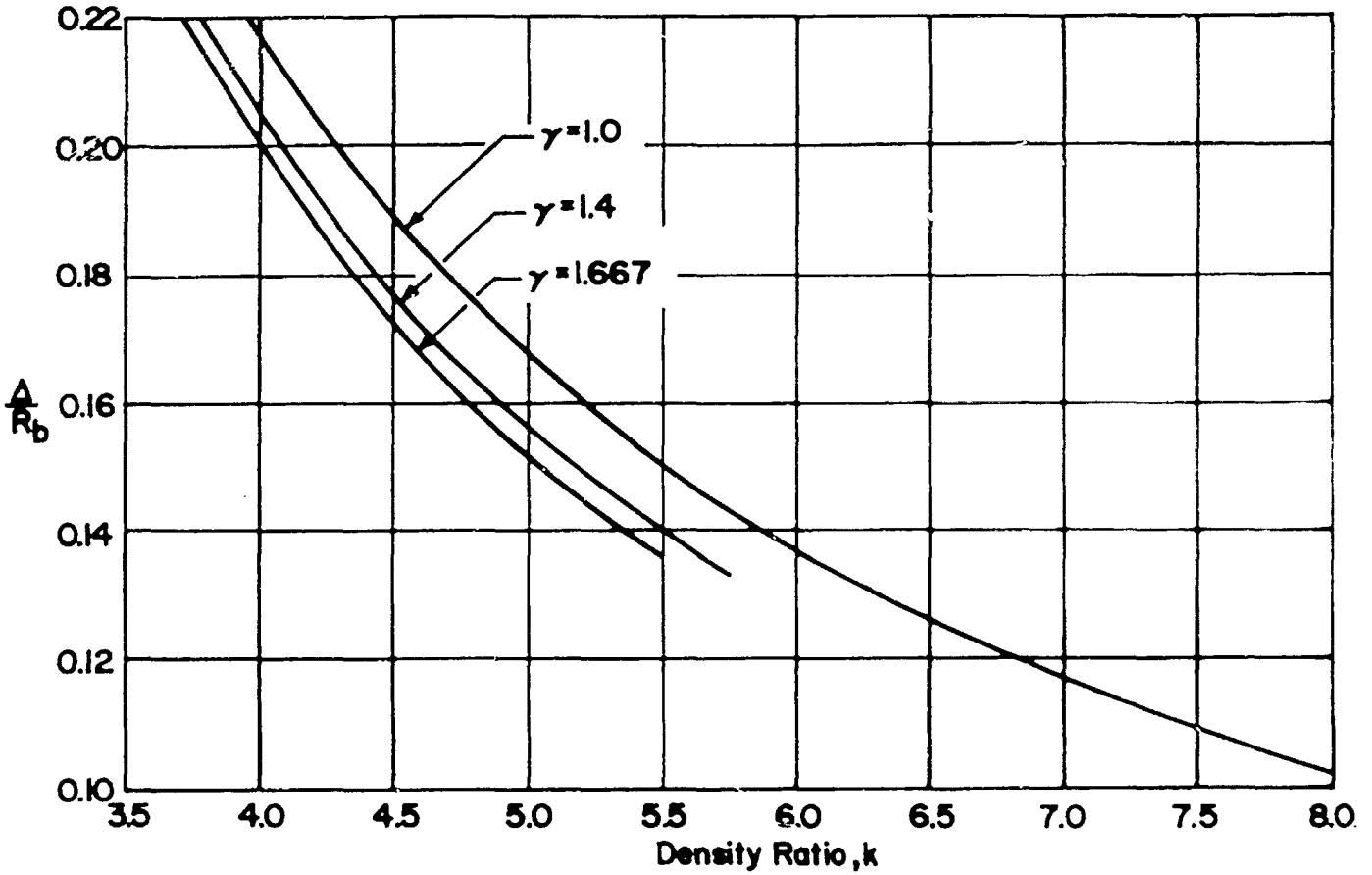

FIGURE 10 - SHOCK DETACHMENT DISTANCE FOR VARYING DENSITY RATIO ACROSS NORMAL PORTION OF BOW SHOCK (REF 8).

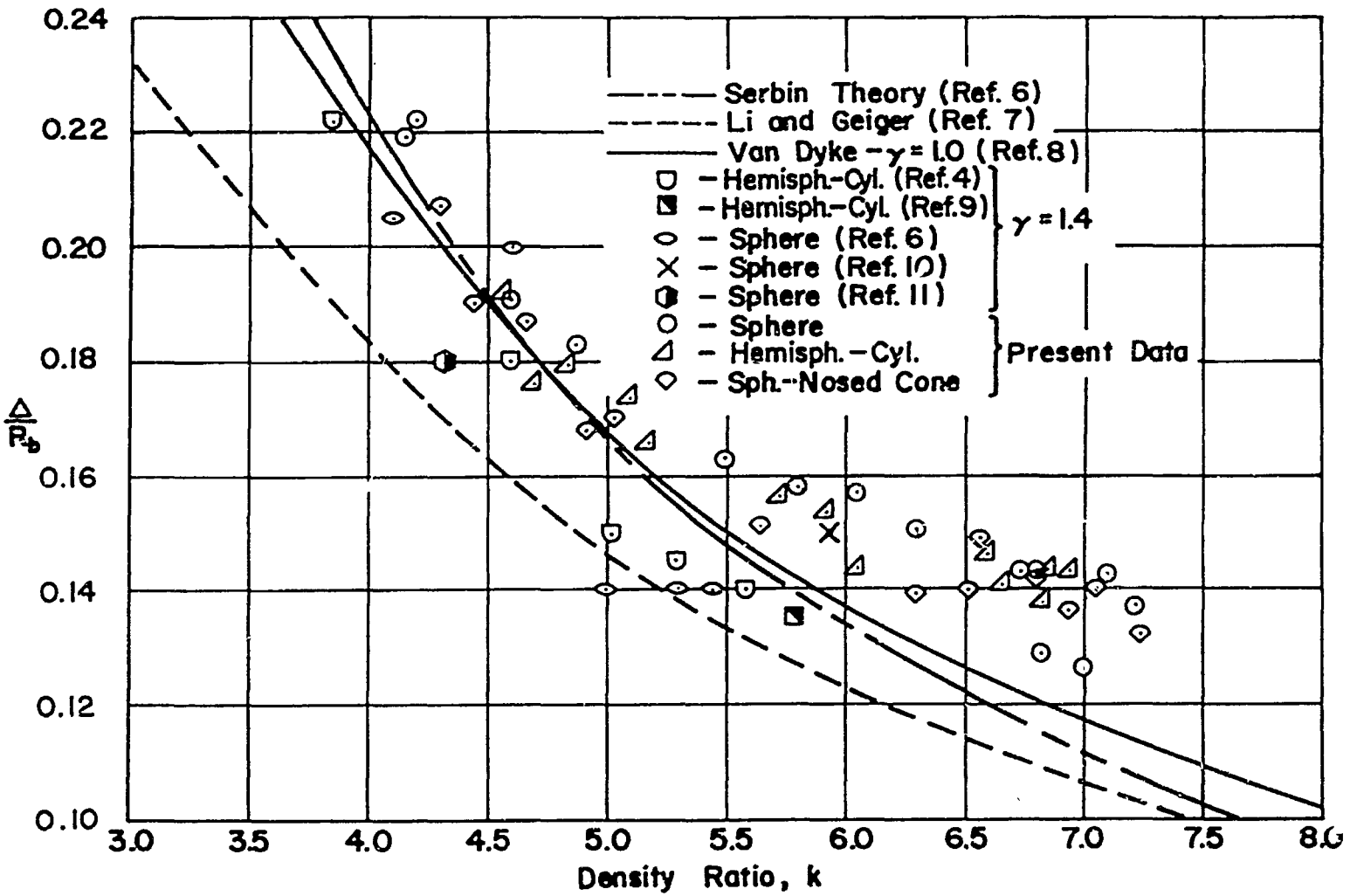

FIGURE 11 — EXPERIMENTAL SHOCK DETACHMENT DISTANCE FOR VARYING EQUILIBRIUM DENSITY RATIO ACROSS NORMAL PORTION OF BOW SHOCK

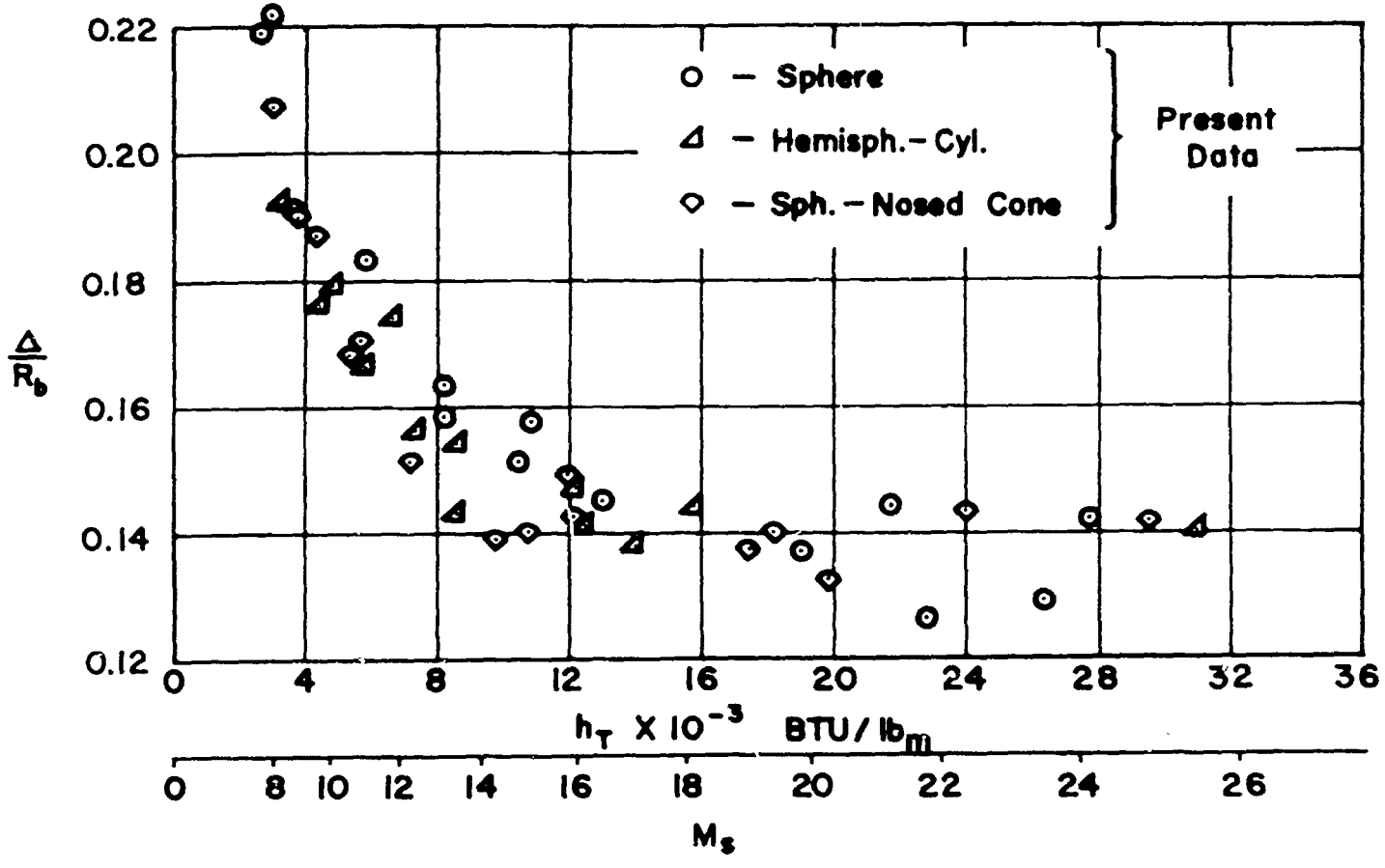

FIGURE 12 — EXPERIMENTAL SHOCK DETACHMENT DISTANCE VERSUS STAGNATION ENTHALPY AND SHOCK MACH NUMBER

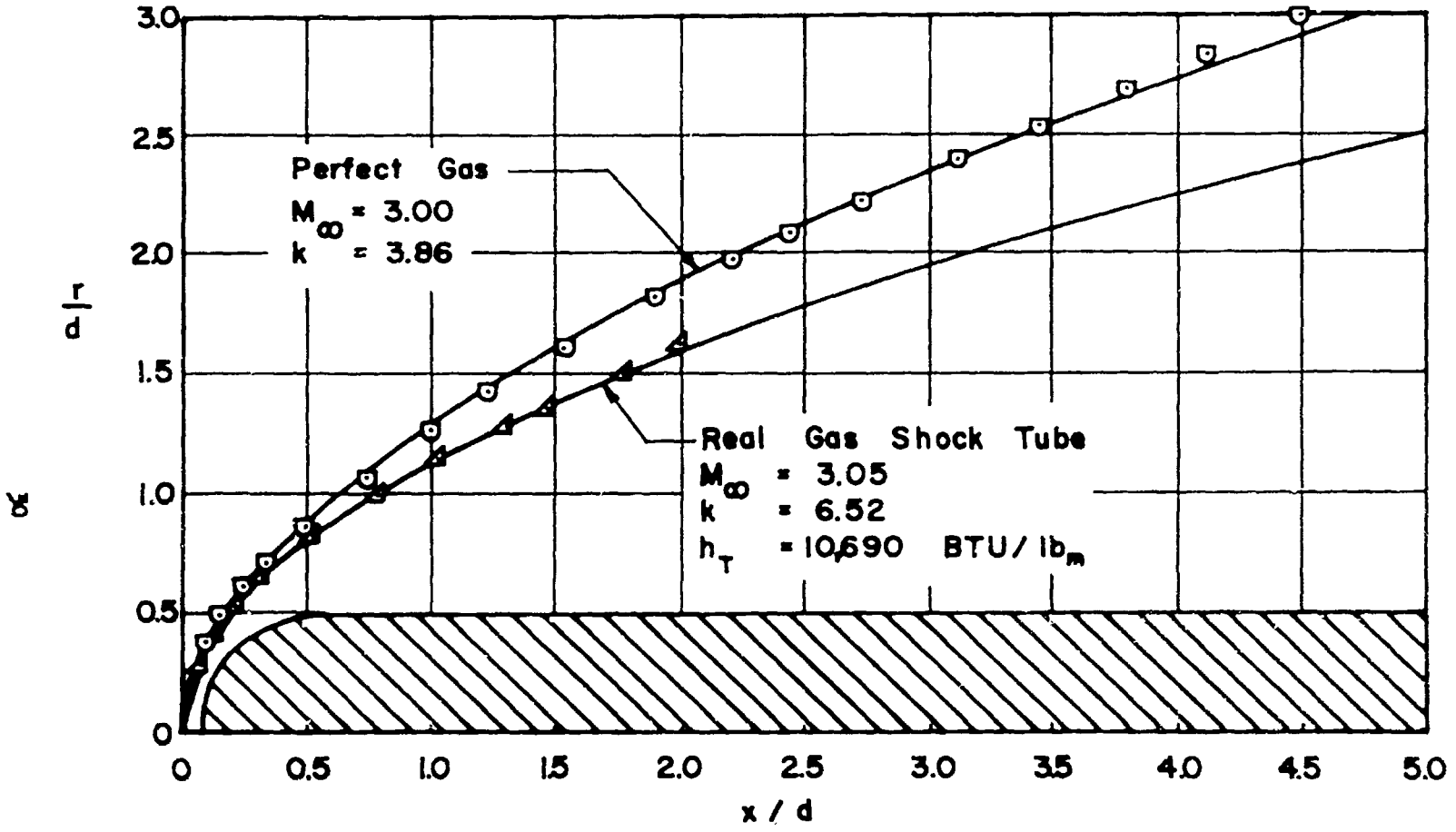

FIGURE 13 — EXPERIMENTAL SHOCK WAVE PROFILES FOR HEMISPHERE CYLINDER

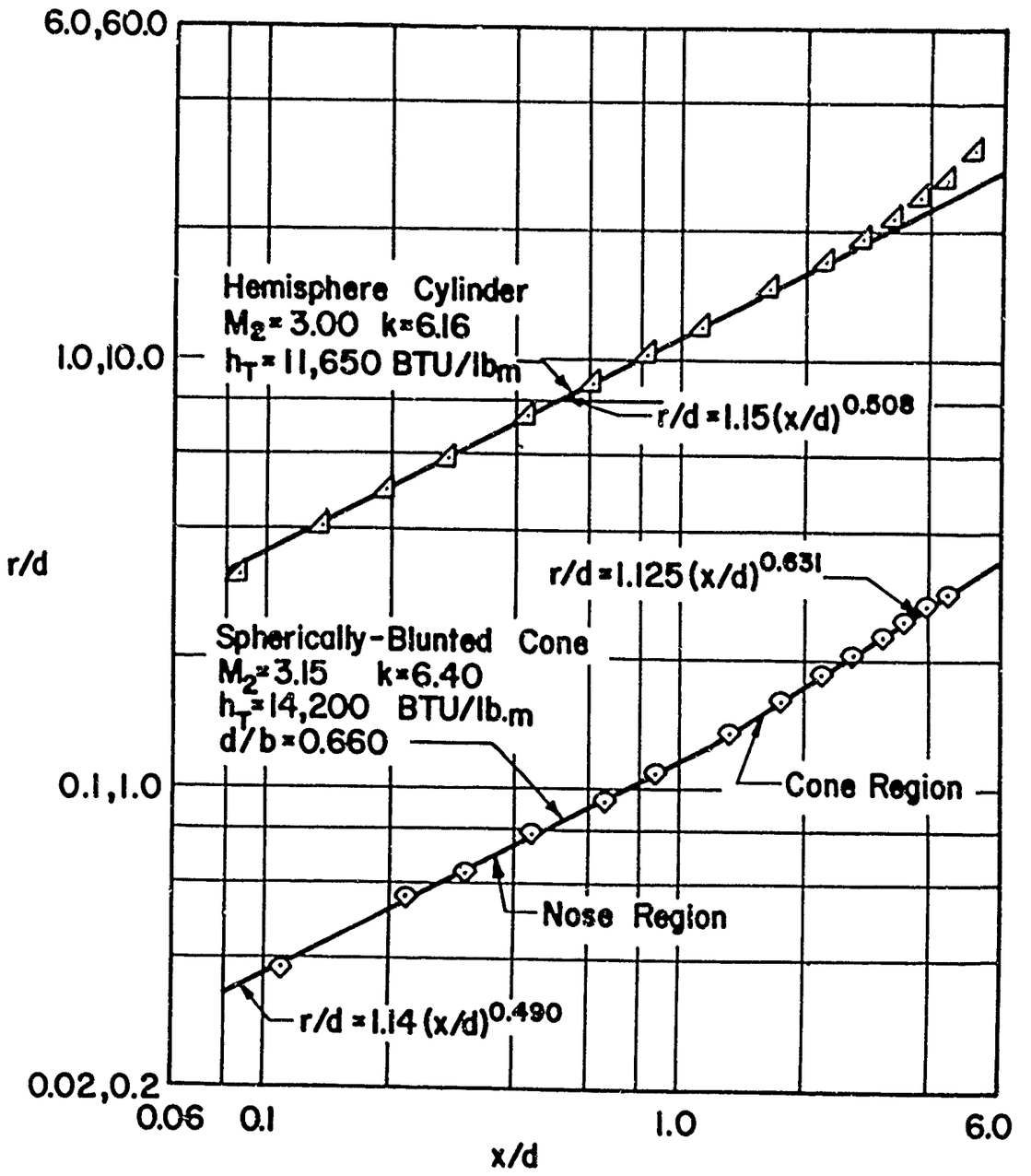

FIGURE 14 - SHOCK WAVE PROFILE FOR HEMISPHERE CYLINDER AND 9 DEGREE HALF-ANGLE, SPHERICALLY BLUNTED CONE

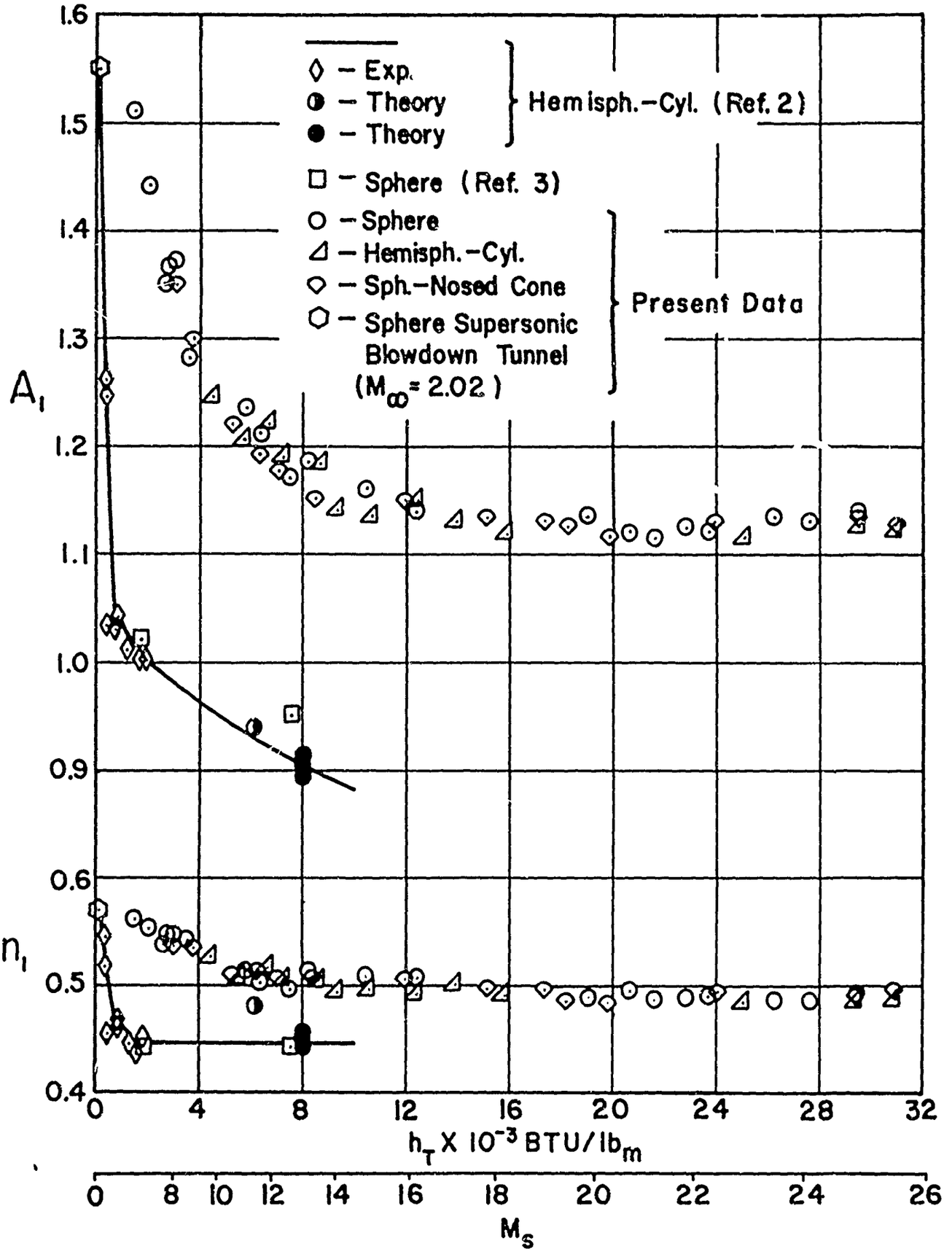

FIGURE 15 — SHOCK WAVE CONSTANTS IN NOSE REGION AS FUNCTION OF STAGNATION ENTHALPY

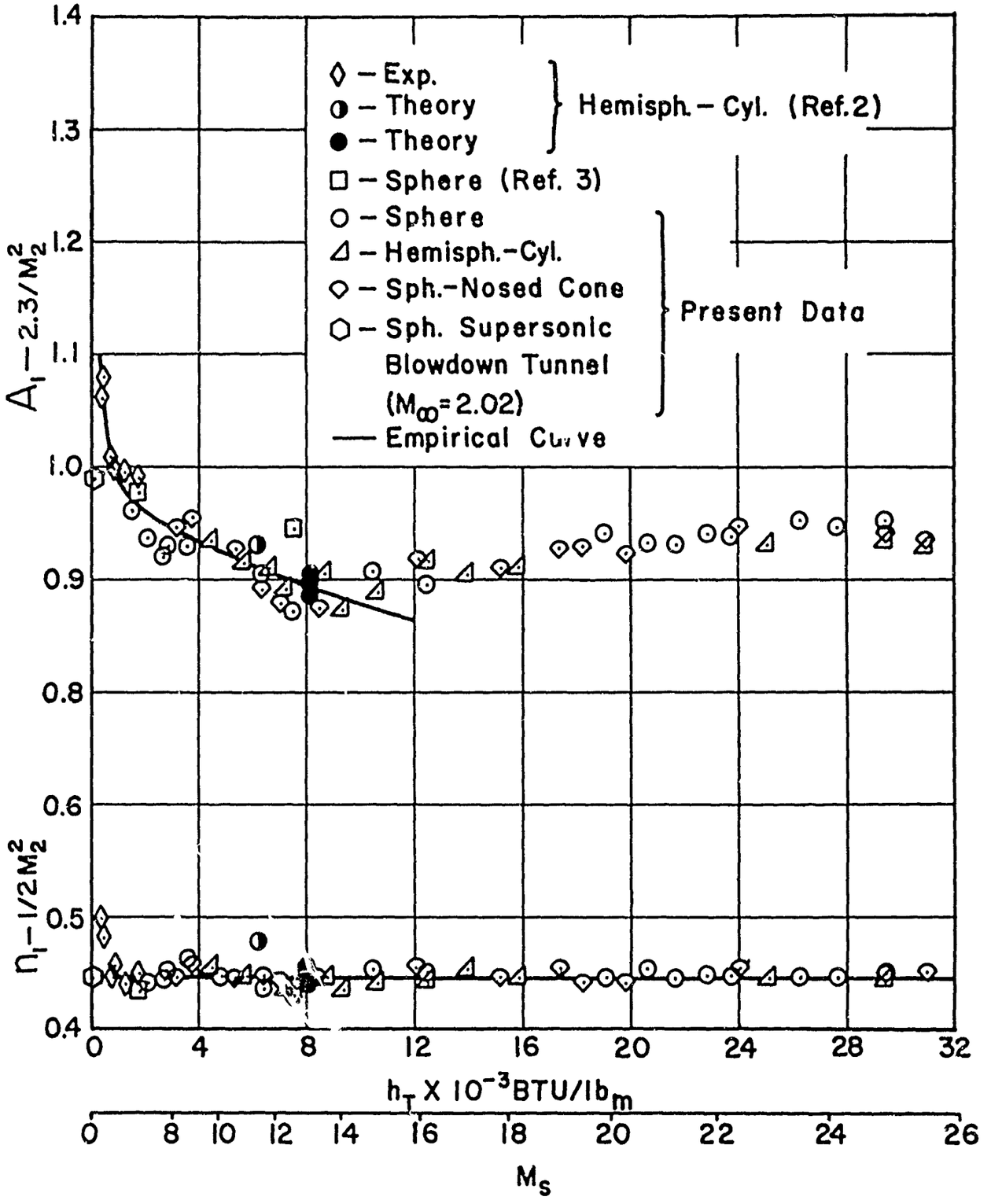

FIGURE 16 — CORRELATION OF NOSE REGION CONSTANTS VERSUS STAGNATION ENTHALPY

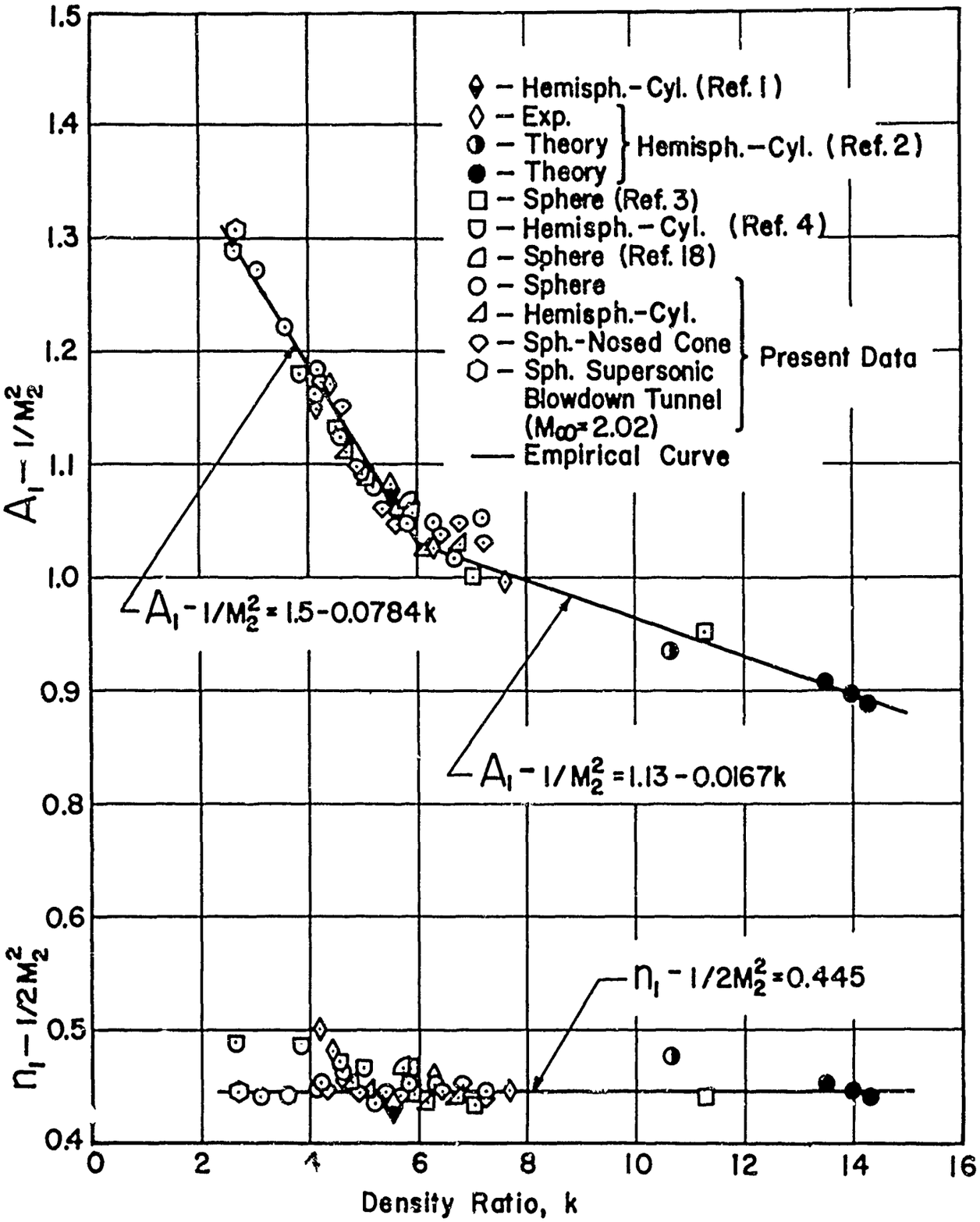

FIGURE 17 — CORRELATION OF NOSE REGION CONSTANTS VERSUS EQUILIBRIUM DENSITY RATIO ACROSS NORMAL PORTION OF BOW SHOCK

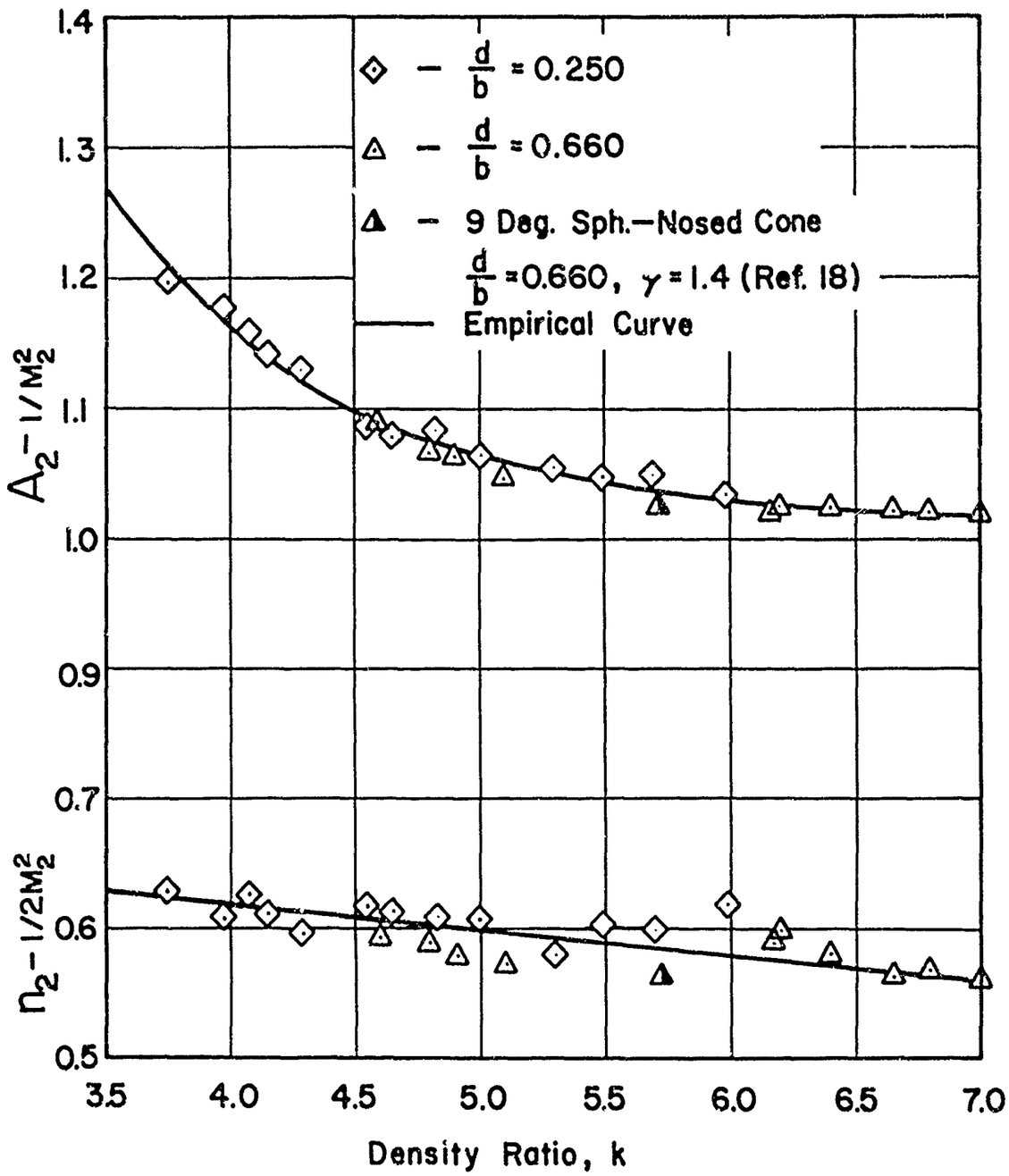

FIGURE 18 — SHOCK WAVE CONSTANTS FOR CONE REGION OF 9 DEGREE HALF-ANGLE, SPHERICALLY BLUNTED CONE VERSUS EQUILIBRIUM DENSITY RATIO ACROSS NORMAL PORTION OF BOW SHOCK

DOCUMENT CONTROL DATA - R&D

(Security classification of title body of abstract and indexing annotation must be entered when the overall report is classified)

1 ORIGINATING ACTIVITY *(Corporate author)*
Ohio State University Research Foundation
Columbus, Ohio

2a REPORT SECURITY CLASSIFICATION
UNCLASSIFIED

2b GROUP
N/A

3 REPORT TITLE
An Experimental Study of Real Gas Effects on Shock Detachment Distances and Shock Shapes for a Family of Blunt Axisymmetric Bodies

4 DESCRIPTIVE NOTES *(Type of report and inclusive dates)*
Final (One of several reports)

5 AUTHOR(S) *(Last name first name initial)*
Graber, Bruce (NMI)

6 REPORT DATE	7a TOTAL NO OF PAGES	7b NO OF REFS
	35	23

8a CONTRACT OR GRANT NO	9a ORIGINATOR'S REPORT NUMBER(S)
Contract Nr AF 33(657)-10416	None
b PROJECT NO 1426	
c Task Nr 142604	9b OTHER REPORT NO(S) *(Any other numbers that may be assigned this report)*
d	FDL TDR 64-130

10 AVAILABILITY/LIMITATION NOTICES
Available through OTS.

11 SUPPLEMENTARY NOTES	12 SPONSORING MILITARY ACTIVITY
	AF Flight Dynamics Laboratory Research and Development Division Wright-Patterson AFB, Ohio

13 ABSTRACT

Shock shapes and detachment distances for a group of spherical-nosed bodies are presented and analyzed in terms of their dependence on several of the flow parameters. The experimental data were obtained by testing the models in an arc-driven shock tube facility which produces a high enthalpy supersonic flow behind the traveling normal shock. With the models mounted in this shock-generated supersonic flow, the free-stream conditions with respect to the model were such that the equilibrium density ration across the bow shock and the free-stream Mach number vary as $3.1 \leq k \leq 7.2$ and $2.1 \leq M_2 \leq 3.45$, respectively. The stagnation enthalpy range for the tests (2,000-31,000 BTU/lb_m) allowed for free-stream dissociation and ionization levels of up to 88.0 per cent and 25.0 percent, respectively. These free-stream conditions are not what is typically experienced in wind tunnels and free flight; thus, the handling of the data is somewhat different than usual in the type of quantities needed in the correlation procedure. It is demonstrated that the density ratio across the bow shock is the important parameter for correlating the nose region shock shapes since this produces agreement between the real gas data and perfect gas data. It is also demonstrated that detachment distance may be dependent on the level of free-stream dissociation while the nose region shock shape shows no dependence whatsoever on the degree of gas dissociation or ionization ahead of or behind the bow shock.

DD FORM 1 JAN 64 1473

14 KEY WORDS	LINK A		LINK B		LINK C	
	ROLE	WT	ROLE	WT	ROLE	WT
Hypersonic Bow Shock Shapes						

INSTRUCTIONS

1. ORIGINATING ACTIVITY: Enter the name and address of the contractor, subcontractor, grantee, Department of Defense activity or other organization *(corporate author)* issuing the report.

2a. REPORT SECURITY CLASSIFICATION. Enter the overall security classification of the report. Indicate whether "Restricted Data" is included. Marking is to be in accordance with appropriate security regulations.

2b. GROUP: Automatic downgrading is specified in DoD Directive 5200.10 and Armed Forces Industrial Manual. Enter the group number. Also, when applicable, show that optional markings have been used for Group 3 and Group 4 as authorized.

3. REPORT TITLE: Enter the complete report title in all capital letters. Titles in all cases should be unclassified. If a meaningful title cannot be selected without classification, show title classification in all capitals in parenthesis immediately following the title.

4. DESCRIPTIVE NOTES: If appropriate, enter the type of report, e.g., interim, progress, summary, annual, or final. Give the inclusive dates when a specific reporting period is covered.

5. AUTHOR(S): Enter the name(s) of author(s) as shown on or in the report. Enter last name, first name, middle initial. If military, show rank and branch of service. The name of the principal author is an absolute minimum requirement.

6. REPORT DATE: Enter the date of the report as day, month, year, or month, year. If more than one date appears on the report, use date of publication.

7a. TOTAL NUMBER OF PAGES: The total page count should follow normal pagination procedures, i.e., enter the number of pages containing information.

7b. NUMBER OF REFERENCES: Enter the total number of references cited in the report.

8a. CONTRACT OR GRANT NUMBER: If appropriate, enter the applicable number of the contract or grant under which the report was written.

8b, 8c, & 8d. PROJECT NUMBER: Enter the appropriate military department identification, such as project number, subproject number, system numbers, task number, etc.

9a. ORIGINATOR'S REPORT NUMBER(S): Enter the official report number by which the document will be identified and controlled by the originating activity. This number must be unique to this report.

9b. OTHER REPORT NUMBER(S). If the report has been assigned any other report numbers *(either by the originator or by the sponsor)*, also enter this number(s).

10. AVAILABILITY/LIMITATION NOTICES: Enter any limitations on further dissemination of the report, other than those imposed by security classification, using standard statements such as:

(1) "Qualified requesters may obtain copies of this report from DDC."

(2) "Foreign announcement and dissemination of this report by DDC is not authorized."

(3) "U. S. Government agencies may obtain copies of this report directly from DDC. Other qualified DDC users shall request through _____."

(4) "U. S. military agencies may obtain copies of this report directly from DDC. Other qualified users shall request through _____."

(5) "All distribution of this report is controlled. Qualified DDC users shall request through _____."

If the report has been furnished to the Office of Technical Services, Department of Commerce, for sale to the public, indicate this fact and enter the price, if known.

11. SUPPLEMENTARY NOTES: Use for additional explanatory notes.

12. SPONSORING MILITARY ACTIVITY: Enter the name of the departmental project office or laboratory sponsoring *(paying for)* the research and development. Include address.

13 ABSTRACT: Enter an abstract giving a brief and factual summary of the document indicative of the report, even though it may also appear elsewhere in the body of the technical report. If additional space is required, a continuation sheet shall be attached.

It is highly desirable that the abstract of classified reports be unclassified. Each paragraph of the abstract shall end with an indication of the military security classification of the information in the paragraph, represented as *(TS), (S), (C), or (U)*

There is no limitation on the length of the abstract. However, the suggested length is from 150 to 225 words.

14 KEY WORDS: Key words are technically meaningful terms or short phrases that characterize a report and may be used as index entries for cataloging the report. Key words must be selected so that no security classification is required. Identifiers, such as equipment model designation, trade name, military project code name, geographic location, may be used as key words but will be followed by an indication of technical context. The assignment of links, rules, and weights is optional.